

Dear Dr. Tsigaridis,

Please see our responses below. All additional changes made to the document use Track Changes. They add to changes that we had made in our initial revision and that we highlight here in yellow.

Sincerely,
Patrick Kim

Editor Initial Decision: Reconsider after major revisions (31 Aug 2015) by Kostas Tsigaridis

Comments to the Author:
Dear authors,

I do not feel that all comments of reviewer #1 have been adequately addressed. In particular:

Major comment #1 is hardly addressed. Paraphrasing the manuscript changes a bit, the new statements of "sulfate increased by 50% which improved the SO₂/sulfate ratio", and "increase in simulated surface PM_{2.5} by 15-25%" are not enough. The reviewer's question was: "It's not clear from the manuscript whether the ability of the model to capture PM concentrations in the Southeast in 2013 is a result of the extensive model modifications and if so, which factor(s) are most important". It appears that only the minor comment #5 has been answered by the text changes.

We have added a paragraph on page 10 that provides a more detailed response to the reviewer's question.

Major comment #3 is also not addressed. The expansion of the discussion in Section 7 mentioned in the reply, is only limited to an addition of a statement in a parenthesis. I understand that the main point is the seasonal cycle of surface PM vs. AOD, however an underestimation of the seasonal cycle itself needs to be discussed, for the reader to be convinced that the model provides an answer for the correct reasons.

We had added some discussion of this in our revision (text highlighted in yellow on p.19). We understand why the model AOD is too low in summer and this is discussed in the paper. We are not sure why the model AOD is too high in winter and can only speculate. In any case, it makes sense that the seasonal variation in PBL height would dampen the seasonal cycle of surface PM compared to AOD, which is what we find in the model and had not been pointed out previously. We have now added a statement to this effect next to the highlighted text.

Major comment #4 is also not properly addressed. The new statement in the abstract, as well as the short new sentence in lines 312-313, are not answering the most interesting part of the reviewer's comment: "Does this study suggest that SOA is non-volatile, and models should eliminate the use of partitioning theory and NO_x-dependent yields?". Even if this is the case only in the SEUS, it is worth mentioning. If not, a statement that speculates on why the model is better with non-volatile SOA should be introduced. Maybe the model behaves as it is, due to the

changes mentioned in major comment #1? Combined with minor comment #4, why only reference Marais et al. 2015, which has the more mechanistic approach, without elaborating on why the two approaches differ, and (if at all possible) recommend on the best one to use?

We had added text in our initial revision to the effect of our work suggesting that SOA is non-volatile (text highlighted in this version). We have now added more text to that effect, provided more detail on the Marais et al. work, and made it clear that Marais et al. has the improved mechanism for isoprene SOA. See our edits on page 9, page 10, and in the Conclusions.

On a last remark, please mention when concluding which results are driven from (and are only applicable to) the SEUS, as opposed to the global scale.

We have added clarifying statements in the conclusion that our results are applicable to the Southeast US. We don't know if they are applicable to the global scale.

Please adequately address the major comments of reviewer #1, as outlined above, and provide a detailed answer and track-changes text that addresses these points.

Kind regards
Kostas Tsigaridis

1 **Sources, seasonality, and trends of Southeast US aerosol: an integrated analysis of surface,**
2 **aircraft, and satellite observations with the GEOS-Chem chemical transport model**

3

4 P. S. Kim¹, D. J. Jacob^{1,2}, J. A. Fisher³, K. Travis², K. Yu², L. Zhu², R. M. Yantosca², M. P.
5 Sulprizio², J. L. Jimenez^{4,5}, P. Campuzano-Jost^{4,5}, K. D. Froyd^{4,6}, J. Liao^{4,6}, J. W. Hair⁷, M. A.
6 Fenn⁸, C. F. Butler⁸, N. L. Wagner^{4,6}, T. D. Gordon^{4,6}, A. Welti^{4,6,9}, P. O. Wennberg^{10,11}, J. D.
7 Crounse¹⁰, J. M. St. Clair^{10,*,**}, A. P. Teng¹⁰, D. B. Millet¹², J. P. Schwarz⁶, M. Z. Markovic^{4,6,***},
8 and A. E. Perring^{4,6}

9

10 ¹Department of Earth and Planetary Sciences, Harvard University, Cambridge, MA, USA

11 ²School of Engineering and Applied Sciences, Harvard University, Cambridge, MA, USA

12 ³School of Chemistry, University of Wollongong, Wollongong, New South Wales, Australia

13 ⁴Cooperative Institute for Research in Environmental Sciences, University of Colorado Boulder,
14 Boulder, Colorado, USA

15 ⁵Department of Chemistry and Biochemistry, University of Colorado Boulder, Boulder,
16 Colorado, USA

17 ⁶Chemical Sciences Division, National Oceanic and Atmospheric Administration Earth System
18 Research Laboratory, Boulder, Colorado, USA

19 ⁷NASA Langley Research Center, Hampton, Virginia, USA

20 ⁸Science Systems and Applications, Inc., Hampton, Virginia, USA

21 ⁹Institute for Atmospheric and Climate Science, Swiss Federal Institute of Technology, Zurich,
22 Switzerland

23 ¹⁰Division of Geological and Planetary Sciences, California Institute of Technology, Pasadena,
24 California, USA

25 ¹¹Division of Engineering and Applied Science, California Institute of Technology, Pasadena,
26 California, USA

27 ¹²Department of Soil, Water, and Climate, University of Minnesota, Minneapolis-Saint Paul, MN,
28 USA

29 *now at: Atmospheric Chemistry and Dynamics Laboratory, NASA Goddard Space Flight Center,
30 Greenbelt, MD, USA

31 **now at: Joint Center for Earth Systems Technology, University of Maryland Baltimore County,
32 Baltimore, MD, USA

33 ***now at: Air Quality Research Division, Environment Canada, Toronto, Ontario, Canada

34

35 Correspondence to: P. S. Kim (kim68@fas.harvard.edu)

36

37 **Abstract**

38

39 We use an ensemble of surface (EPA CSN, IMPROVE, SEARCH, AERONET), aircraft
40 (SEAC⁴RS), and satellite (MODIS, MISR) observations over the Southeast US during the
41 summer-fall of 2013 to better understand aerosol sources in the region and the relationship
42 between surface particulate matter (PM) and aerosol optical depth (AOD). The GEOS-Chem
43 global chemical transport model (CTM) with 25 x 25 km² resolution over North America is used
44 as a common platform to interpret measurements of different aerosol variables made at different
45 times and locations. Sulfate and organic aerosol (OA) are the main contributors to surface PM_{2.5}
46 (mass concentration of PM finer than 2.5 μm aerodynamic diameter) and AOD over the Southeast
47 US. OA is simulated successfully with a simple parameterization assuming irreversible uptake of
48 low-volatility products of hydrocarbon oxidation. Biogenic isoprene and monoterpenes account
49 for 60% of OA, anthropogenic sources for 30%, and open fires for 10%. 60% of total aerosol
50 mass is in the mixed layer below 1.5 km, 25% in the cloud convective layer at 1.5-3 km, and 15%
51 in the free troposphere above 3 km. This vertical profile is well captured by GEOS-Chem,
52 arguing against a high-altitude source of OA. The extent of sulfate neutralization ($f =$
53 $[\text{NH}_4^+]/(2[\text{SO}_4^{2-}] + [\text{NO}_3^-])$) is only 0.5-0.7 mol mol⁻¹ in the observations, despite an excess of
54 ammonia present, which could reflect suppression of ammonia uptake by OA. This would explain
55 the long-term decline of ammonium aerosol in the Southeast US, paralleling that of sulfate. The
56 vertical profile of aerosol extinction over the Southeast US follows closely that of aerosol mass.
57 GEOS-Chem reproduces observed total column aerosol mass over the Southeast US within 6%,
58 column aerosol extinction within 16%, and space-based AOD within 8-28% (consistently biased
59 low). The large AOD decline observed from summer to winter is driven by sharp declines in both
60 sulfate and OA from August to October. These declines are due to shutdowns in both biogenic
61 emissions and UV-driven photochemistry. Surface PM_{2.5} shows far less summer-to-winter
62 decrease than AOD and we attribute this in part to the offsetting effect of weaker boundary layer
63 ventilation. The SEAC4RS aircraft data demonstrate that AODs measured from space are
64 consistent with surface PM_{2.5}. This implies that satellites can be used reliably to infer surface
65 PM_{2.5} over monthly timescales if a good CTM representation of the aerosol vertical profile is
66 available.

67

68

Daniel Jacob 8/31/2015 10:18 PM

Formatted: Highlight

Daniel Jacob 8/31/2015 10:11 PM

Deleted: due

70 **1. Introduction**

71

72 There is considerable interest in using satellite retrievals of aerosol optical depth (AOD)
73 to map particulate matter concentrations (PM) in surface air and their impact on public health (Y.
74 Liu et al., 2004; H. Zhang et al., 2009; van Donkelaar et al., 2010, 2015; X. Hu et al., 2014). The
75 relationship between PM and AOD is a function of the vertical distribution and optical properties
76 of the aerosol. It is generally derived from a global chemical transport model (CTM) simulating
77 the different aerosol components over the depth of the atmospheric column (van Donkelaar et al.,
78 2012, 2013; Boys et al., 2014). Sulfate and organic matter are the dominant submicron aerosol
79 components worldwide (Murphy et al., 2006; Q. Zhang et al., 2007; Jimenez et al., 2009), thus it
80 is important to evaluate the ability of CTMs to simulate their concentrations and vertical
81 distributions. Here we use the GEOS-Chem CTM to interpret a large ensemble of aerosol
82 chemical and optical observations from surface, aircraft, and satellite platforms during the NASA
83 SEAC⁴RS campaign in the Southeast US in August-September 2013. Our objective is to better
84 understand the relationship between PM and AOD, and the ability of CTMs to simulate it, with
85 focus on the factors controlling sulfate and organic aerosol (OA).

86 The Southeast US is a region of particular interest for PM air quality and for aerosol
87 radiative forcing of climate (Goldstein et al., 2009). PM_{2.5} (the mass concentration of particulate
88 matter finer than 2.5 μm aerodynamic diameter, of most concern for public health) is in
89 exceedance of the current US air quality standard, 12 $\mu\text{g m}^{-3}$ on an annual mean basis, in several
90 counties (<http://www.epa.gov/airquality/particlepollution/actions.html>). Concentrations have been
91 decreasing in response to regulation targeted at protecting public health (the Clean Air Act
92 Amendments of 1990). Figure 1 shows the summertime (JJA) and wintertime (DJF) mean
93 concentrations of aerosol components for 2003-2013 from surface monitoring stations in the
94 Southeast US managed by the US Environmental Protection Agency (US EPA, 1999).
95 Summertime sulfate concentrations decreased by 60% over the period while OA concentrations
96 decreased by 40% (Hand et al., 2012b; Blanchard et al., 2013; Hidy et al., 2014). Trends in
97 winter are much weaker. Decreasing aerosol has been linked to rapid warming in the Southeast
98 US over the past two decades (Leibensperger et al., 2012ab).

99 The sulfate decrease is driven by the decline of sulfur dioxide (SO₂) emissions from coal
100 combustion (Hand et al., 2012b), though the mechanisms responsible for oxidation of SO₂ to
101 sulfate are not well quantified. Better understanding of the mechanisms is important because dry
102 deposition competes with oxidation as a sink of SO₂, so that faster oxidation produces more
103 sulfate (Chin and Jacob, 1996). Standard model mechanisms assume that SO₂ is oxidized to

104 sulfate by the hydroxyl radical (OH) in the gas phase and by hydrogen peroxide (H₂O₂) and ozone
105 in clouds (aqueous phase). A model intercomparison by McKeen et al. (2007) for the Northeast
106 US revealed a general failure of models to reproduce observed sulfate concentrations, sometimes
107 by a factor of 2 or more. This could reflect errors in oxidation mechanisms, oxidant
108 concentrations, or frequency of cloud processing. Laboratory data suggest that stabilized Criegee
109 intermediates (SCIs) formed from alkene ozonolysis could be important SO₂ oxidants (Mauldin et
110 al., 2012; Welz et al., 2012), though their ability to produce sulfate may be limited by competing
111 reactions with water vapor (Chao et al., 2015; Millet et al., 2015).

112 The factors controlling OA are highly uncertain. OA originates from anthropogenic,
113 biogenic, and open fire sources (de Gouw and Jimenez, 2009). It is directly emitted as primary
114 OA (POA) and also produced in the atmosphere as secondary OA (SOA) from oxidation of
115 volatile organic compounds (VOCs). Current models cannot reproduce observed OA variability,
116 implying fundamental deficiencies in the model mechanisms (Heald et al., 2011; Spracklen et al.,
117 2011; Tsigaridis et al., 2014). A key uncertainty for air quality policy is the fraction of OA that
118 can be controlled (Carlton et al., 2010), as most of the carbon in SOA is thought to be biogenic in
119 origin. Gas/particle partitioning of organic material depends on the pre-existing aerosol
120 concentration (Pankow et al., 1994; Donahue et al., 2006), so that “biogenic” SOA may be
121 enhanced in the presence of anthropogenic POA and SOA (Weber et al., 2007). The SOA yield
122 from VOC oxidation also depends on the concentration of nitrogen oxide radicals (NO_x = NO +
123 NO₂) (Kroll et al., 2005, 2006; A. Chan et al. 2010; Hoyle et al., 2011; Xu et al., 2014). NO_x in
124 the Southeast US is mostly from fossil fuel combustion and is in decline due to emission controls
125 (Russell et al., 2012), adding another complication in the relationship between OA concentrations
126 and anthropogenic sources. Oxidation of biogenic VOC by the NO₃ radical formed from
127 anthropogenic NO_x is also thought to be an important SOA source in the Southeast US (Pye et al.
128 2010). Reactions of organic molecules with sulfate to form organosulfates may also play a small
129 role (Surratt et al., 2007; Liao et al., 2015).

130 Long-term PM_{2.5} records for the Southeast US are available from the EPA CSN,
131 IMPROVE, and SEARCH networks of surface sites (Malm et al., 1994; Edgerton et al., 2005;
132 Solomon et al., 2014). Satellite measurements of AOD from the MODIS and MISR instruments
133 have been operating continuously since 2000 (Diner et al., 2005; Remer et al., 2005; Levy et al.,
134 2013). Both surface and satellite observations show a strong aerosol seasonal cycle in the
135 Southeast US, with a maximum in summer and minimum in winter (Alston et al., 2012; Hand et
136 al., 2012a; Ford and Heald, 2013). Goldstein et al. (2009) observed that the amplitude of the
137 seasonal cycle of PM_{2.5} measured at surface sites (maximum/minimum ratio of ~1.5; Hand et al.,

138 2012a) is much smaller than the seasonal cycle of AOD measured from space (ratio of ~3-4;
139 Alston et al., 2012). They hypothesized that this could be due to a summertime source of biogenic
140 SOA aloft. Subsequent work by Ford and Heald (2013) supported that hypothesis on the basis of
141 spaceborne CALIOP lidar measurements of elevated light extinction above the planetary
142 boundary layer (PBL).

143 The NASA SEAC⁴RS aircraft campaign in August-September 2013 (Toon et al., 2015)
144 offers a powerful resource for better understanding the factors controlling aerosol concentrations
145 in the Southeast US and the relationship between surface PM and AOD measured from space.
146 The aircraft payload included measurements of aerosol composition, size distribution, and light
147 extinction along with a comprehensive suite of aerosol precursors and related chemical tracers.
148 Flights provided dense coverage of the Southeast US (Figure 2) including extensive PBL
149 mapping and vertical profiling. AERONET sun photometers deployed across the region provided
150 AOD measurements (Holben et al., 1998; http://aeronet.gsfc.nasa.gov/new_web/dragon.html).
151 Additional field campaigns focused on Southeast US air quality during the summer of 2013
152 included SENEX (aircraft) and NOMADSS (aircraft) based in Tennessee (Warneke et al., 2015;
153 http://www.eol.ucar.edu/field_projects/nomadss), DISCOVER-AQ (aircraft) based in Houston
154 (Crawford and Pickering, 2014), SOAS (surface) based in Alabama (<http://soas2013.rutgers.edu>),
155 and SLAQRS (surface) based in Greater St. Louis (Baasandorj et al., 2015). We use the GEOS-
156 Chem CTM with 0.25° x 0.3125° horizontal resolution as a platform to exploit this ensemble of
157 observational constraints by (1) determining the consistency between different measurements, (2)
158 interpreting the measurements in terms of their implications for the sources of sulfate and OA in
159 the Southeast US, (3) explaining the seasonal aerosol cycle in the satellite and surface data, and
160 (4) assessing the ability of CTMs to relate satellite measurements of AOD to surface PM.

161

162 **2. The GEOS-Chem CTM**

163

164 GEOS-Chem has been used extensively to simulate aerosol concentrations over the US
165 including comparisons to observations (Park et al., 2003, 2004, 2006; Drury et al., 2010; Heald et
166 al., 2011, 2012; Leibensperger et al., 2012a; Walker et al., 2012; L. Zhang et al., 2012; Ford and
167 Heald, 2013). Here we use GEOS-Chem version 9-02 (<http://geos-chem.org>) with detailed
168 oxidant-aerosol chemistry and the updates described below. Our SEAC⁴RS simulation for
169 August-October 2013 is driven by Goddard Earth Observing System – Forward Processing
170 (GEOS-FP) assimilated meteorological data from the NASA Global Modeling and Assimilation
171 Office (GMAO). The GEOS-FP meteorological data have a native horizontal resolution of 0.25°

172 x 0.3125° (~25 x 25 km²) with 72 vertical pressure levels and 3 h temporal frequency (1 h for
173 surface variables and mixed layer depths). The mixed layer (ML) is defined in GEOS-FP as the
174 unstable surface-based column diagnosed from the potential temperature gradient, with a vertical
175 resolution of ~150 m. It is used in GEOS-Chem for surface-driven vertical mixing following Lin
176 and McElroy (2010). The representation of clouds and their properties, such as liquid water
177 content, are taken from the GEOS-FP assimilated meteorological fields. We use the native
178 resolution in GEOS-Chem over North America and adjacent oceans [130° - 60° W, 9.75° - 60° N]
179 to simulate the August 1 – October 31, 2013 period with a 5-minute transport time step. This is
180 nested within a global simulation at 4° x 5° horizontal resolution to provide dynamic boundary
181 conditions. The global simulation is initialized on June 1, 2012 with climatological model fields
182 and spun up for 14 months, effectively removing the sensitivity to initial conditions.

183 GEOS-Chem simulates the mass concentrations of all major aerosol components
184 including sulfate, nitrate, and ammonium (SNA; Park et al., 2006; L. Zhang et al., 2012), organic
185 carbon (OC; Heald et al., 2006a, 2011; Fu et al., 2009), black carbon (BC; Q. Wang et al., 2014),
186 dust in four size bins (Fairlie et al., 2007), and sea salt in two size bins (Jaegle et al., 2011).
187 Aerosol chemistry is coupled to HO_x-NO_x-VOC-O₃-BrO_x tropospheric chemistry with recent
188 updates to the isoprene oxidation mechanism as described by Mao et al. (2013). Gas/particle
189 partitioning of SNA aerosol is computed with the ISORROPIA II thermodynamic module
190 (Fontoukis and Nenes, 2007), as implemented in GEOS-Chem by Pye et al. (2009). Aerosol wet
191 and dry deposition are described by H. Liu et al. (2001) and L. Zhang et al. (2001) respectively.
192 OC is the carbon component of OA, and we infer simulated OA from OC by assuming OA/OC
193 mass ratios for different OC sources as given by Canagaratna et al. (2015). Model results are
194 presented below either as OC or OA depending on the measurement to which they are compared.
195 Measurements from surface networks are as OC while the aircraft measurements are as OA.

196 Table 1 lists GEOS-Chem emissions in the continental United States (CONUS) for 2013.
197 Values for the Southeast US in August-September are in parentheses. Emissions outside the
198 CONUS are as in Kim et al. (2013) and are used in the global simulation to derive the boundary
199 conditions for the nested grid. US anthropogenic emissions are from the EPA National Emissions
200 Inventory for 2010 (NEI08v2). The NEI emissions are mapped over the 0.25° x 0.3125° GEOS-
201 Chem grid and scaled to the year 2013 by the ratio of national annual totals
202 (<http://www.epa.gov/ttnchie1/trends/>). For BC and SO₂ this implies 3% and 10% decreases from
203 2010 to 2013, but we prescribe instead a 30% decrease for both to better match observed BC
204 concentrations and trends in sulfate wet deposition. Our SO₂ emission adjustment is more
205 consistent with the latest version of the EPA inventory (NEI11v1), which indicates a 34% decline

206 between 2010 and 2013, and with the observed trend in surface concentrations from the SEARCH
207 network, which indicates a ~50% decline in the Southeast US over the same years (Hidy et al.,
208 2014). The NEI08 NH₃ emissions are scaled to 2° x 2.5° gridded monthly totals from the
209 MASAGE inventory, which provides a good simulation of ammonium wet deposition in the US
210 (Paulot et al., 2014).

211 Open fires have a pervasive influence on OA and BC over the US (Park et al., 2007).
212 During SEAC⁴RS, the Southeast US was affected by both long-range transport of smoke from
213 wildfires in the West (Peterson et al., 2014; Saide et al., 2015) and local agricultural fires. We use
214 the Quick Fire Emissions Dataset (QFED2; Darmenov and da Silva, 2013), which provides daily
215 open fire emissions at 0.1° x 0.1° resolution. Diurnal scale factors, which vary by an order of
216 magnitude between midday and evening and peak at 10-19 local time, are applied to the QFED2
217 daily emissions following recommendations from the Western Regional Air Partnership (WRAP,
218 2005) as in Saide et al. (2015). Following previous results from Turquety et al. (2007) and
219 Fischer et al. (2014) for extratropical fires, we inject 35% of fire emissions above the boundary
220 layer between 680 and 450 hPa to account for plume buoyancy.

221 Biogenic VOC emissions are from the MEGAN2.1 inventory of Guenther et al. (2012)
222 implemented in GEOS-Chem as described by Hu et al. (2015). Isoprene emissions are decreased
223 by 15% to better match SEAC⁴RS observations of isoprene and formaldehyde concentrations and
224 surface fluxes (Travis et al., 2015; Wolfe et al., 2015; Zhu et al., 2015). Figure 2 shows the
225 SEAC⁴RS DC-8 flight tracks superimposed on the distribution of isoprene emissions. Total
226 emissions over the Southeast US (domain outlined in Figure 2) during the 2-month SEAC⁴RS
227 period were 2.2 Tg C for isoprene and 0.5 Tg C for monoterpenes. Monoterpene emissions did
228 not exceed isoprene emission anywhere.

229 Sulfate was too low in our initial simulations of the SEAC⁴RS observations. We
230 addressed this problem by including SCIs as additional SO₂ oxidants in the model as previously
231 implemented in GEOS-Chem by Pierce et al. (2013). Oxidation of isoprene and monoterpenes
232 provides a large source of SCIs in the Southeast US in summer. Sipila et al. (2014) estimated SCI
233 molar yields from ozonolysis of 0.58 ± 0.26 from isoprene, 0.15 ± 0.07 from α-pinene, and 0.27
234 ± 0.12 from limonene. Sarwar et al. (2014) previously found that simulation of sulfate with the
235 CMAQ CTM compared better with summertime surface observations in the Southeast US when
236 SCI + SO₂ reactions were included in the chemical mechanism. However, production of sulfate
237 from SCI chemistry may be severely limited by competition for SCIs between SO₂ and water
238 vapor and depends on the respective reaction rate constants (Welz et al., 2012; J. Li et al., 2013;
239 Newland et al., 2014; Sipila et al., 2014; Stone et al., 2014). Here we use SCI chemistry from the

Daniel Jacob 8/31/2015 11:49 AM

Moved down [1]: This increased mean sulfate over the Southeast US by 50% and improved simulation of the SO₂/sulfate ratio (Section 4).

243 Master Chemical Mechanism (MCMv3.2; Jenkins et al., 1997; Saunders et al., 2003) with the
244 SCI + SO₂ and SCI + H₂O rate constants from Stone et al. (2014), using CH₂OO as a proxy for
245 all SCIs, such that the SCI + SO₂ pathway dominates. This would not be the case using the
246 standard SCI + H₂O and significantly slower (~1000x) SCI + SO₂ rate constants in MCM (Millet
247 et al., 2015) or if reaction with the water vapor dimer is important (Chao et al., 2015). Given
248 these crude approximations coupled with the uncertain SCI kinetics, the simulated SCI
249 contribution to SO₂ oxidation can be viewed as a proxy for missing oxidant or insufficient cloud
250 processing in GEOS-Chem.

251 A number of mechanisms of varying complexity have been proposed to model OA
252 chemistry (Donahue et al., 2006; Henze et al., 2006; Ervens et al., 2011; Spracklen et al., 2011;
253 Murphy et al., 2012; Barsanti et al., 2013; Hermansson et al., 2014). These mechanisms tend to
254 be computationally expensive and have little success in reproducing the observed variability of
255 OA concentrations (Tsigaridis et al., 2014). Here we use a simple linear approach to simulate five
256 components of OA – anthropogenic POA and SOA, open fire POA and SOA, and biogenic SOA.
257 Anthropogenic and open fire POA emissions are from the NEI08 and QFED2 inventories
258 described above. For anthropogenic and open fire SOA, we adopt the Hodzic and Jimenez (2011)
259 empirical parameterization that assumes irreversible condensation of the oxidation products of
260 VOC precursor gases (AVOC and BBVOC respectively). AVOCs and BBVOCs are emitted in
261 proportion to CO, with an emission ratio of 0.069 g AVOC (g CO)⁻¹ (Hayes et al., 2014) and
262 0.013 g BBVOC (g CO)⁻¹ (Cubison et al., 2011). They are both oxidized by OH in the model with
263 a rate constant of 1.25 x 10⁻¹¹ cm³ molecule⁻¹ s⁻¹ to generate SOA. This approach produces
264 amounts of SOA and timescales of formation consistent with field measurements at many
265 locations (de Gouw and Jimenez, 2009; Hodzic and Jimenez, 2010; Cubison et al., 2011; Jolleys
266 et al., 2012; Hayes et al., 2014).

267 We assume biogenic SOA to be produced with a yield of 3% from isoprene and 5% from
268 monoterpenes, formed at the point of emission. Laboratory studies have shown that different
269 biogenic SOA formation mechanisms operate depending on the NO concentration, which
270 determines the fate of the organic peroxy radicals (RO₂) produced from VOC oxidation (Kroll et
271 al., 2005, 2006; A. Chan et al., 2010; Xu et al., 2014). In the high-NO pathway the RO₂ radicals
272 react with NO, while in the low-NO pathway they react with HO₂, other RO₂ radicals, or
273 isomerize. During SEAC⁴RS the two pathways were of comparable importance (Travis et al.,
274 2015). We use four separate tracers in the model to track SOA formed from isoprene and
275 monoterpenes via the high- and low-NO pathways. This tracer separation is purely diagnostic as
276 the SOA yields are assumed here to be the same in both pathways. The SOA is apportioned to the

Daniel Jacob 8/31/2015 12:35 PM

Deleted: The standard semi-volatile partitioning treatment of OA in GEOS-Chem v9.02 (Pye et al., 2010) underestimates SEAC⁴RS observations several-fold.

281 high- or low-NO tracer by the fraction of RO₂ reacting with NO at the point and time of emission.
282 A more mechanistic GEOS-Chem simulation of isoprene SOA in SEAC⁴RS including
283 irreversible aqueous-phase formation coupled to gas-phase chemistry is presented by Marais et al.
284 (2015). It finds in particular that the mean isoprene SOA yield in the low-NO pathway is twice
285 that in the high-NO pathway.

286 GEOS-Chem computes the AOD for each aerosol component i by summing the optical
287 depths over all vertical model layers $L = [1, \dots, n]$:

288

$$289 \quad \text{AOD} = \sum_i \sum_{L=1}^n \alpha_i(L) M_i(L) \quad [1]$$

290

291 where $\alpha_i(L)$ and $M_i(L)$ are respectively the component mass extinction efficiency ($\text{m}^2 \text{g}^{-1}$) and
292 partial column mass (g m^{-2}) for level L . The α_i values are pre-calculated for selected wavelengths
293 using a standard Mie scattering algorithm. The algorithm assumes specified aerosol dry size
294 distributions and optical properties from the Global Aerosol Data Set (GADS; Koepke et al.,
295 1997), with updates by Drury et al. (2010) on the basis of summer observations from the ICARTT
296 aircraft campaign over the eastern US. The mass extinction efficiencies are then adjusted for
297 hygroscopic growth as a function of the local relative humidity (RH), following R. Martin et al.
298 (2003). The total AOD is reported here at 550 nm and is the sum of the contributions from all
299 aerosol components. Comparison of dry aerosol size distribution and hygroscopic growth show
300 good general agreement with observations similar to Drury et al. (2010) (Supplementary
301 Material).

302 Comparison of GEOS-FP ML heights with lidar and ceilometer data from SEAC⁴RS,
303 SOAS, and DISCOVER-AQ indicates a 30-50% positive bias across the Southeast US in daytime
304 (Scarino et al., 2014b; Millet et al., 2015). We decrease the daytime GEOS-FP ML heights by
305 40% in our simulation to correct for this bias. During SEAC⁴RS, ML heights were measured by
306 the NASA-Langley High Spectral Resolution Lidar (HSRL; Hair et al., 2008, Scarino et al.,
307 2014a) on the basis of aerosol gradients under clear-sky conditions. After correction, the modeled
308 ML height is typically within 10% of the HSRL data along the SEAC⁴RS flight tracks, with a
309 mean daytime value (± 1 standard deviation) of 1690 ± 440 m in the HSRL data and 1530 ± 330
310 m in the model (Zhu et al., 2015). The daytime ML was typically capped by a shallow cloud
311 convective layer (CCL) extending up to about 3 km, capped in turn by a subsidence inversion and
312 the free troposphere above. When giving column statistics we will refer to the ML as below 1.5
313 km and the CCL as between 1.5 and 3 km.

Daniel Jacob 9/2/2015 3:27 PM

Deleted: NO_x-dependent yields and comparison to semi-volatile partitioning theory is reported

Daniel Jacob 9/2/2015 2:21 PM

Deleted: This increases simulated surface PM_{2.5} by 15-25%.

318 Our simulation of sulfate and OA differs in a number of ways from previous GEOS-
319 Chem simulations using earlier versions of the model (Park et al., 2004, 2006; Heald et al.,
320 2006a; Leibensperger et al., 2012; Zhang et al., 2012; Ford and Heald, 2013). Benchmark
321 simulations of ²¹⁰Pb aerosol (Liu et al., 2001;
322 http://acmg.seas.harvard.edu/geos/geos_benchmark.html) show that the global mean aerosol
323 lifetime against deposition is 15% shorter with the GEOS-FP meteorological data used here than
324 with the previously used GEOS-5 data. Correcting the ML height bias over the Southeast US in
325 the GEOS-FP data increases our simulated PM_{2.5} concentrations by 15-25%. Previous GEOS-
326 Chem studies did not include the Criegee biradical mechanism for SO₂ oxidation, which in our
327 simulation increases the mean sulfate concentrations over the Southeast US by 50% and increases
328 the SO₂/sulfate ratio to better agree with observations (Section 4). The default SOA mechanism in
329 GEOS-Chem, based on reversible partitioning of semivolatile products of VOC oxidation (Pye et
330 al., 2010), underestimates OA levels during SEAC⁴RS by a factor of 3 (Marais et al., 2015). The
331 simple SOA parameterization used here effectively assumes irreversible uptake as a mechanism
332 for SOA formation and provides a much improved simulation of OA over the Southeast US, as
333 shown below. Marais et al. (2015) present a more mechanistic treatment of isoprene SOA
334 formation in GEOS-Chem, based on irreversible uptake in aqueous aerosols, in their simulation
335 of SEAC⁴RS observations. Their mean SOA yield from isoprene (3.3%) is comparable to our
336 imposed value of 3% but accounts for NO_x dependence.

337 Several companion papers apply the same GEOS-Chem model configuration as described
338 here to other analyses of the SEAC⁴RS data focused on gas-phase chemistry. These include
339 investigation of the factors controlling ozone in the Southeast US (Travis et al., 2015), isoprene
340 chemistry and the formation of organic nitrates (Fisher et al., 2015), validation of satellite HCHO
341 data as constraints on isoprene emissions (Zhu et al., 2015), and sensitivity of model
342 concentrations and processes to grid resolution (K. Yu et al., 2015). These studies include
343 extensive comparisons to the gas-phase observations in SEAC⁴RS. Our focus here will be on the
344 aerosol observations.

345

346 3. Surface Aerosol Concentrations

347

348 We begin by evaluating the simulation of PM_{2.5} and its components against ground
349 observations. Total PM_{2.5} is measured gravimetrically at 35% RH at a large number of EPA
350 monitoring sites (Figure 3). Filter-based measurements of PM_{2.5} composition are taken every
351 three days at surface networks including the EPA CSN (25 sites in the study domain marked in

Daniel Jacob 8/31/2015 11:49 AM

Moved (insertion) [1]

Daniel Jacob 8/31/2015 10:05 PM

Deleted: This increased

Daniel Jacob 9/1/2015 2:07 PM

Deleted: improved simulation of

354 Figure 2, mostly in urban areas), IMPROVE (15 sites, mostly in rural areas), and SEARCH (5
355 sites, urban and suburban/rural). These three networks all provide 24-h average concentrations of
356 the major ions (SNA), carbon species (BC and OC), and dust, though there are differences in
357 protocols (Edgerton et al., 2005; Hidy et al., 2014; Solomon et al., 2014), in particular with
358 respect to OC artifact correction. The IMPROVE and SEARCH OC are both blank-corrected but
359 in different ways (Dillner et al., 2009; Chow et al., 2010), while CSN OC is uncorrected. We
360 apply a constant $0.3 \mu\text{g m}^{-3}$ background correction to the CSN OC data as in Hand et al. (2012a).
361 The resulting CSN OC measurements are within 1% of SEARCH and 44% higher than
362 IMPROVE when averaged across the Southeast US. When necessary, OA is inferred from the OC
363 filter samples using an OA/OC mass ratio of 2.24 as measured in the boundary layer during
364 SEAC⁴RS by an aerosol mass spectrometer (AMS) onboard the DC-8 aircraft (Section 4). We do
365 not discuss sea-salt concentrations as they make a negligible contribution to $\text{PM}_{2.5}$ inland (< 0.1
366 $\mu\text{g m}^{-3}$ averaged across the EPA networks).

367 Figure 3 shows mean August-September 2013 $\text{PM}_{2.5}$ at the EPA sites and compares to
368 GEOS-Chem values. Concentrations peak over Arkansas, Louisiana, and Mississippi,
369 corresponding to the region of maximum isoprene emission in Figure 2. The spatial distribution
370 and composition of $\text{PM}_{2.5}$ is otherwise fairly homogeneous across the Southeast US, reflecting
371 coherent stagnation, mixing, and ventilation of the region (X. Zhang et al., 2012; Pfister et al.,
372 2015). Sulfate accounts on average for 25% of $\text{PM}_{2.5}$ while OA accounts for 55%. GEOS-Chem
373 captures the broad features shown in the surface station $\text{PM}_{2.5}$ data with little bias ($R = 0.65$,
374 normalized mean bias or NMB = -1.4%). The model hotspot in southern Arkansas is due to OA
375 from a combination of biogenic emissions and agricultural fires. As discussed below, agricultural
376 fires make only a small contribution on a regional scale.

377 The spatial distributions of sulfate and OC concentrations are shown in Figure 4. The
378 observed and simulated sulfate maxima are shifted to the northeast relative to total $\text{PM}_{2.5}$ shown
379 in Figure 3. GEOS-Chem captures a larger fraction of the observed variability at rural sites ($R =$
380 0.78 for IMPROVE) than at urban/suburban sites ($R = 0.71$ for SEARCH, 0.62 for CSN) as
381 would be expected from the sub-grid scale of urban pollution. A scatterplot of the simulated daily
382 mean surface sulfate concentrations compared to the filter observations from all three networks in
383 August-September 2013 is shown in the Supplementary Material. The model bias (NMB) is +5%
384 relative to IMPROVE, +10% relative to SEARCH, and +9% relative to CSN. Over the Southeast
385 US domain defined in Figure 2, 42% of sulfate production is from in-cloud production by H_2O_2 ,
386 22% is from gas-phase oxidation by OH, and 36% is from gas-phase oxidation by SCIs. Previous
387 studies by Pierce et al. (2013) and Boy et al. (2013) found similarly large contributions of SCIs to

388 sulfate production over forested regions in summer. However, there is substantial uncertainty in
389 the SCI kinetics, as discussed above, and it is possible that other oxidants are responsible for the
390 missing sulfate (hence the “Other” label in Figure 4).

391 The observed OC distribution shows a decreasing gradient from southwest to northeast
392 that maps onto the distribution of isoprene emissions shown in Figure 2. The IMPROVE OC is
393 generally low compared to CSN and SEARCH, as has been noted previously (Ford and Heald,
394 2013; Attwood et al., 2014). GEOS-Chem reproduces the broad features of the observed OC
395 distribution with moderate skill in capturing the variability ($R = 0.64$ for IMPROVE, 0.62 for
396 SEARCH, 0.61 for CSN). Model OC is biased high with a NMB of +66% for IMPROVE, +29%
397 for SEARCH, and +14% for CSN. The range of NMBs for the different networks could reflect
398 differences in measurement protocols described above - IMPROVE OC is lower than SEARCH
399 by 27% for collocated measurements made at Birmingham, Alabama (Supplementary Material).
400 We discuss this further in the next section in the context of the aircraft data.

401 Source attribution of OC in the model (Figure 4) suggests a dominance of biogenic
402 sources. Isoprene alone contributes 42% of the regional OC burden. This is in contrast with
403 previous work by Barsanti et al. (2013), who fitted chamber observations to a model mechanism
404 and found monoterpenes to be as or more important than isoprene as a source of OC in the
405 Southeast US (particularly under low-NO conditions). SEAC⁴RS observations support a
406 significant role of isoprene as a source of OA (W. Hu et al., 2015; Campuzano-Jost et al., 2015;
407 Liao et al., 2015).

408 Anthropogenic sources in the model contribute 28% to regional OC, roughly evenly
409 distributed across the region. Open fires contribute 11%, mainly from agricultural fires in
410 Arkansas and Missouri. Influence from western US fires is significant in the free troposphere (see
411 Section 4) but not at the surface.

412 When all of the components are taken together, we find that 81% of the surface OC in the
413 Southeast US is secondary in origin. This is well above the 30-69% range of previous literature
414 estimates for the region (Lim and Turpin, 2002; S. Yu et al., 2004; Kleindienst et al., 2007;
415 Blanchard et al., 2008) and likely reflects the decreasing trend in anthropogenic emissions (Figure
416 1) and possibly a low bias in some estimation methods (Docherty et al., 2008). Assuming fossil
417 fractions of 50% and 70% for anthropogenic primary and secondary OC respectively (Zotter et
418 al., 2014; Hayes et al. 2014), we estimate that 18% of the total OC burden is derived from fossil
419 fuel use. This is consistent with an 18% fossil fraction from radiocarbon measurements made on
420 filter samples collected in Alabama during SOAS (Edgerton et al., 2014).

421

422 4. Aerosol Vertical Profile

423

424 We now examine the aerosol vertical distribution measured by the NASA DC-8 aircraft
425 and simulated by GEOS-Chem along the flight tracks on 18 flights over the Southeast US (Figure
426 2). Aerosol mass composition was measured by a High-Resolution Aerodyne AMS for SNA and
427 OA (Canagaratna et al., 2007) and by the NOAA humidified dual single-particle soot photometer
428 for BC (HD-SP2; Schwarz et al., 2015). Dust concentrations were measured from filter samples
429 (Dibb et al., 2003), but the ML values are $\sim 10\times$ higher than measured by surface networks or
430 simulated in GEOS-Chem, as previously found by Drury et al. (2010) during ICARTT. Instead
431 we estimate dust concentrations from Particle Analysis by Laser Mass Spectrometer (PALMS)
432 measurements (Thomson et al., 2000; Murphy et al., 2006). The PALMS data provide the size-
433 resolved number fraction of dust-containing particles, which is multiplied by the measured
434 aerosol volume size distribution from the LAS instrument (Thornhill et al., 2008; Chen et al.,
435 2011) and an assumed density of 2.5 g cm^{-3} . The size distribution is truncated to $\text{PM}_{2.5}$ by
436 applying the transmission curve for the $2.5 \text{ }\mu\text{m}$ aerosol impactor used by the ground networks.

437 Figure 5 shows the median sulfate, OA, and dust vertical profiles over the Southeast US.
438 Also shown are the median concentrations from the surface networks over the study domain
439 shown in Figure 2. The difference between the surface and aircraft data that can be attributed to
440 differences in sampling (time and duration) is quantified by the difference in GEOS-Chem output
441 when the model is sampled with the surface data vs. when the model is sampled with the aircraft
442 data. For sulfate, the model underestimates the aircraft observations by 20% below 5 km but
443 overestimates the surface observations by 5-10% as discussed in Section 3. The general shape of
444 the vertical profile is well simulated (with a low bias from 3 to 4 km) and this applies also to SO_2
445 and to the $\text{SO}_2/\text{sulfate}$ ratio (Supplementary Material). The sulfate concentrations are highest near
446 the surface and drop rapidly with altitude, but there is significant mass loading in the lower free
447 troposphere. 23% of the observed sulfate column mass lies in the free troposphere above 3 km
448 and this is well simulated by the model (23%). Analysis of SENEX and SEAC⁴RS vertical
449 profiles by Wagner et al. (2015) suggests that most of this free tropospheric sulfate is ventilated
450 from the PBL rather than being produced within the free troposphere from ventilated SO_2 . GEOS-
451 Chem shows moderate skill in explaining the variability in the aircraft sulfate data ($R = 0.81$ for
452 all observations in the Southeast US, $R = 0.68$ below 3 km, $R = 0.49$ above 3 km).

453 Similarly to sulfate, OA measured from aircraft peaks at the surface and decreases rapidly
454 with height (Figure 5). The aircraft OA mass concentration below 1 km is 25-50% higher than
455 measured at the surface networks. IMPROVE is substantially lower than the other networks, as

456 has been noted above and in previous studies (Ford and Heald, 2013; Attwood et al., 2014), and
457 may be due to instrumental issues particular to that network. The discrepancy between the AMS
458 observations and CSN/SEARCH can largely be explained by differences in sampling, as shown
459 by the model. The GEOS-Chem simulation matches closely the aircraft observations. The vertical
460 distribution of OA is similar to that of sulfate, with 20% of the total column being above 3 km
461 both in the model and in the observations. The GEOS-Chem source attribution, also shown in
462 Figure 5, indicates that open fires contribute ~50% of OA in the free troposphere. This fire
463 influence is seen in the observations as occasional plumes of OA up to 6-7 km altitude (individual
464 gray dots in Figure 5). Fire plumes can be problematic for interpreting the AOD/PM relationship
465 for individual scenes but much less so in a temporal average as the mean influence on the column
466 is small. Simulating fire influence successfully in the model does require buoyant injection of
467 western US wildfire emissions in the free troposphere, as noted in previous studies (Turquety et
468 al., 2007; Fischer et al., 2014).

469 Comparison of GEOS-Chem to the individual OA observations along the aircraft flight
470 tracks shows good simulation of the variability ($R = 0.82$ for all observations, $R = 0.74$ below 3
471 km, $R = 0.42$ above 3 km). This is despite (or maybe because of) our use of a very simple
472 parameterization for the OA source. Further GEOS-Chem comparison to SEAC⁴RS and SOAS
473 observations is presented by Marais et al. (2015) using a more mechanistic analysis of SOA. The
474 successful GEOS-Chem simulation of the OA vertical profile argues against a large CCL source
475 from aqueous-phase cloud processing. This is supported by the work of Wagner et al. (2015),
476 who found little OA enhancement in air masses processed by cumulus wet convection.

477 Dust made only a minor contribution to total aerosol mass in the Southeast US during
478 SEAC⁴RS, accounting for less than 10% of observed surface $PM_{2.5}$ (Figure 3). The PBL dust
479 concentrations measured by PALMS are roughly consistent with the surface data but the model is
480 much lower (Figure 5). This reflects a southward bias in the model transport of Saharan dust
481 (Fairlie et al., 2007), but is of little consequence for the simulation of $PM_{2.5}$ or the AOD/PM
482 relationship over the Southeast US. Figure 5 shows few free tropospheric plumes in the
483 SEAC⁴RS observations, consistent with the dust climatology compiled from CALIOP data by D.
484 Liu et al. (2008).

485 Figure 6 compiles the median observed and simulated vertical profiles of aerosol
486 concentrations and composition during SEAC⁴RS. OA and sulfate dominate at all altitudes.
487 Ammonium is associated with sulfate as discussed in the next Section. OA accounts for most of
488 $PM_{2.5}$ below 1 km, with a mass fraction $F_{OA} = [OA]/[PM_{2.5}]$ of 0.62 g g^{-1} (0.65 in GEOS-Chem).
489 This is consistent with the surface SEARCH data ($F_{OA} = 0.56 \text{ g g}^{-1}$). Figure 1 shows a lower F_{OA}

490 in the IMPROVE surface observations, increasing from 0.34 g g⁻¹ in 2003 to 0.44 g g⁻¹ in 2013,
491 reflecting instrumentation bias as discussed above. The aircraft data show that most of the aerosol
492 mass is OA at all altitudes. The aerosol column is mostly in the PBL (60% in the ML, ~25% in
493 the CCL), but ~15% is in the free troposphere with 10% above 5 km (Figure 6, right panel).
494 GEOS-Chem reproduces the observed shape of the vertical distribution of total aerosol mass, and
495 this is an important result for application of the model to derive the AOD/PM relationship.

496

497 **5. Extent of Neutralization of Sulfate Aerosol**

498

499 The extent of neutralization of sulfate aerosol by ammonia, computed from the fraction f
500 = $[\text{NH}_4^+]/(2[\text{SO}_4^{2-}] + [\text{NO}_3^-])$ where concentrations are molar, has important implications for the
501 aerosol phase and hygroscopicity, for the formation of aerosol nitrate (S. Martin et al., 2004; J.
502 Wang et al., 2008), and for the formation of SOA (Froyd et al., 2010; Eddingsaas, et al., 2012;
503 McNeill et al., 2012; Budisulistiorini et al., 2013; Liao et al., 2015). Figure 6 shows ammonium
504 to be the third most important aerosol component by mass in the Southeast US in summer after
505 OA and sulfate. Summertime particle-phase ammonium concentrations have declined at
506 approximately the same rate as sulfate from 2003 to 2013 (Figure 1 and Blanchard et al., 2013).
507 However, we find no significant trend over that time in ammonium wet deposition fluxes over the
508 Southeast US (National Atmospheric Deposition Program, 2015), in contrast to a ~50% decline in
509 sulfate wet deposition. This implies that ammonia emissions have not decreased but the
510 partitioning into the aerosol has.

511 One would expect ammonium aerosol trends to follow those of sulfate if the aerosol is
512 fully neutralized ($f = 1$), so that partitioning of ammonia into the aerosol phase is limited by the
513 supply of sulfate. However, this is not the case in the observations. Figure 7 shows the extent of
514 neutralization in the observations and the model assuming that the SNA aerosol is externally
515 mixed from other ionic aerosol components such as dust. The model aerosol is fully neutralized
516 ($f = 1$) but the observed aerosol is not, with a median extent of neutralization of 0.55 mol mol⁻¹ in
517 the CSN data and 0.68 mol mol⁻¹ in the AMS data below 2 km. This is comparable to $f = 0.49$
518 mol mol⁻¹ observed at the SOAS Centreville site earlier in the summer. The CSN data include full
519 ionic analysis and we examined whether internal mixing of SNA aerosol with other ions could
520 affect the extent of neutralization. The top right panel of Figure 7 shows that it does not,
521 reflecting the low concentrations of these other ions. The AMS reports total sulfate. While
522 organosulfates have a low pK_a and would interact with ammonium as a single charged ion, they
523 were typically a small fraction of total sulfate (Liao et al., 2015).

524 A possible explanation is that ammonia uptake by aerosol with $f < 1$ may be inhibited by
525 organic particle material. This has been demonstrated in a laboratory study by Liggio et al.
526 (2011), who show that the time constant for ammonia to be taken up by sulfate aerosol with
527 incomplete extent of neutralization increases with the ratio of condensing organic gases to sulfate
528 and may be hours to days.

529 The complete extent of neutralization of sulfate aerosol in the model, in contrast to the
530 observations, leads to bias in the simulated aerosol phase and hygroscopicity for relating AOD to
531 PM. Calculations by J. Wang et al. (2008) for ammonium-sulfate particles of different
532 compositions show a 10-20% sensitivity of the mass extinction efficiency to the extent of
533 neutralization, with the effect changing sign depending on composition and RH. An additional
534 effect of $f = 1$ in the model would be to allow formation of ammonium nitrate aerosol, but nitrate
535 aerosol is negligibly small in the model as it is in the observations (Figure 6). At the high
536 temperatures over the Southeast US in the summer, we find in the model that the product of
537 HNO_3 and NH_3 partial pressures is generally below the equilibrium constant for formation of
538 nitrate aerosol. By contrast, surface network observations in winter show nitrate to be a large
539 component of surface $\text{PM}_{2.5}$ (Figure 1; Hand et al., 2012b; Ford and Heald, 2013), reflecting both
540 lower temperatures and the lower levels of sulfate.

541

542 **6. Aerosol Extinction and Optical Depth**

543

544 We turn next to light extinction measurements onboard the DC-8 to better understand the
545 relationship between the vertical profiles of aerosol mass (Section 4) and AOD. Aerosol
546 extinction coefficients were measured on the SEAC⁴RS aircraft remotely above and below the
547 aircraft by the NASA HSRL and at the altitude of the aircraft by the in situ NOAA cavity
548 ringdown spectrometer (CRDS; Langridge et al., 2011). Figure 8 compares the two
549 measurements, both at 532 nm, with GEOS-Chem. Though the two instruments sampled different
550 regions of the atmosphere at any given time, the mission median profiles are similar. The
551 exception is between 2 and 4 km where the HSRL extinction coefficient is lower. The shapes of
552 the vertical extinction profiles are consistent with aerosol mass (Figure 6). The fraction of total
553 column aerosol extinction below 3 km is 93% for the HSRL data (91% in GEOS-Chem when
554 sampled at the observation times) and 85% for the CRDS data (85% in GEOS-Chem). Almost all
555 of the column extinction is below 5 km (94% for the CRDS and 93% for GEOS-Chem).
556 Integrated up to the ceiling of the DC-8 aircraft, the median AODs from HSRL and the CRDS are
557 0.14 and 0.17 respectively (0.12 and 0.15 for GEOS-Chem).

558 Figure 9 shows maps of the mean AOD over the Southeast US in August-September
559 2013 as measured by AERONET, MISR, MODIS on the Aqua satellite, and simulated by GEOS-
560 Chem. The model is sampled at the local satellite overpass times (1030 for MISR and 1330 for
561 MODIS). We use the Version 31 Level 3 product from MISR (gridded averages at $0.5^\circ \times 0.5^\circ$
562 resolution) and the Collection 6 Level 3 product from MODIS (gridded averages at $1^\circ \times 1^\circ$
563 resolution). We exclude MODIS observations with cloud fraction greater than 0.5 or AOD greater
564 than 1.5 to account for cloud contamination and sensor saturation as in Ford and Heald (2013).
565 We use the Level 2 cloud-filtered daytime average AERONET observations, which can be
566 viewed as a reference measurement.

567 Comparison of daily collocated MODIS and MISR retrievals with AERONET
568 observations shows high correlation and little bias (statistics inset in Figure 9). These statistics
569 were calculated only when there are collocated and corresponding data for both AERONET and
570 the satellite retrieval, whereas Figure 9 shows the spatial average of all available data during
571 August-September 2013. MODIS shows a broad maximum over the Southeast US that
572 corresponds well with observed $PM_{2.5}$ in Figure 3. There is greater heterogeneity in the MISR
573 average due to sparse sampling. GEOS-Chem captures the spatial pattern of the regional AOD
574 enhancement when sampled with the different retrievals and underestimates the magnitude by
575 16% (NMB relative to AERONET), consistent with the underestimate of the aircraft aerosol
576 extinction data (including the NASA Ames 4STAR sun photometer, Supplementary Material).
577 The model underestimates AOD (NMB) by 28% relative to MODIS and by 8% relative to MISR.

578

579 **7. The Aerosol Seasonal Cycle**

580

581 As pointed out in the introduction, there has been considerable interest in interpreting the
582 aerosol seasonal cycle over the Southeast US and the difference in seasonal amplitude between
583 AOD and surface $PM_{2.5}$ (Goldstein et al. 2009, Ford and Heald, 2013). Figure 10 shows MODIS
584 monthly average AOD over the Southeast US for 2006-2013. The observed AOD in 2013 shows
585 a seasonal cycle consistent with previous years. There has been a general decline in the seasonal
586 amplitude over 2006-2013 driven by a negative summertime trend, with 2011 being anomalous
587 due to high fire activity. The same long-term decrease and 2011 anomaly are seen in the surface
588 $PM_{2.5}$ data (Figure 1). Examination of Figure 10 reveals that the entirety of the seasonal decrease
589 from summer to winter takes place as a sharp transition in the August-October window, in all
590 years.

591 We analyzed the causes of this August-October transition using the GEOS-Chem
592 simulation of the SEAC⁴RS period. Figure 11 (panel A) shows the time series of daily median
593 AOD from AERONET, GEOS-Chem sampled at the times and locations of the AERONET
594 observations, and MODIS over the Southeast US. The difference between AERONET and
595 MODIS can be explained by differences in sampling (they otherwise correspond well with each
596 other, see Section 6). Observations through early September show large oscillations with a 7-10
597 day period driven by frontal passages. These are well reproduced by the model. The observed
598 AODs then fall sharply in mid-September and again this is well reproduced by GEOS-Chem. The
599 successful simulation of the August-October seasonal transition implies that we can use the
600 model to understand the causes of this transition. Figure 11 also shows the sulfate and OA
601 contributions to GEOS-Chem AOD. Sulfate aerosol contributes as much to column light
602 extinction as OA, despite lower concentrations, due to its higher mass extinction efficiency. Both
603 the sulfate and OA contributions to AOD fall during the seasonal transition.

604 We find that the sharp drops in sulfate and OA concentrations over August-October are
605 due to two factors. The first is a decline in isoprene and monoterpene emissions due to cooler
606 surface temperatures and leaf senescence (panel B of Figure 11). The second is a transition in the
607 photochemical regime as UV radiation sharply declines (Kleinman, 1991; Jacob et al., 1995),
608 depleting OH and H₂O₂ (panel C) and hence sulfate formation.

609 The seasonal transition in photochemical regime also involves a shift from a low-NO to a
610 high-NO chemical regime (Kleinman, 1991; Jacob et al., 1995). This would affect the SOA yield
611 (Marais et al., 2015), though this is not represented in the current GEOS-Chem simulation. Panel
612 D of Figure 11 shows the ratio of isoprene hydroperoxides (ISOPOOH) to isoprene nitrate
613 (ISOPN) concentrations measured in the PBL during SEAC⁴RS by the Caltech CIMS (Crouse et
614 al., 2006; St. Clair et al., 2010) and simulated by GEOS-Chem. ISOPOOH is formed under low-
615 NO conditions, while ISOPN is formed under high-NO conditions. Both observations and the
616 model show a decline in the ISOPOOH/ISOPN concentration ratio over the course of SEAC⁴RS,
617 with the model showing extended decline into October. If the SOA yield is higher under low-NO
618 conditions (Kroll et al., 2005, 2006; Xu et al. 2014) then this would also contribute to the
619 seasonal decline in OA.

620 We have thus explained the seasonality of AOD as driven by aerosol sources. Previous
621 studies have pointed out that surface PM_{2.5} in the Southeast US has much weaker seasonality than
622 AOD, and observed PM_{2.5} in 2013 had no significant seasonality (Figure 12, top panel). This
623 difference in the amplitude of the seasonal cycle between PM_{2.5} and AOD is simulated to some
624 extent by GEOS-Chem, as shown in Figure 12. It is driven in GEOS-Chem by the seasonal

Daniel Jacob 8/31/2015 10:14 PM

Deleted: also

626 variation in ML height (middle panel of Figure 12), dampening the seasonal cycle of PM_{2.5} by
627 reducing ventilation in winter. The AOD in GEOS-Chem is lower than observed in summer and
628 higher in winter, so that the seasonality is weaker than observed (a factor of 2 compared to an
629 observed factor of 3-4). The summer underestimate is consistent with the aircraft observations, as
630 discussed previously. The winter overestimate could reflect seasonal error in model aerosol
631 sources or optical properties. These model biases aside, one would expect the seasonal variation
632 of boundary layer mixing to dampen the seasonal variation of surface PM_{2.5} relative to AOD, as is
633 found in the observations and in the model.

Daniel Jacob 8/31/2015 10:16 PM
Formatted: Highlight

635 8. Conclusions

636
637 We have used a large ensemble of surface, aircraft, and satellite observations during the
638 SEAC⁴RS field campaign over the Southeast US in August-September 2013 to better understand
639 (1) the sources of sulfate and organic aerosol (OA) in the region; (2) the relationship between the
640 aerosol optical depth (AOD) measured from space and the fine particulate matter concentration
641 (PM_{2.5}) measured at the surface; and (3) the seasonal aerosol cycle and the apparent inconsistency
642 between satellite and surface measurements. Our work used the GEOS-Chem global chemical
643 transport model (CTM) with 0.25° x 0.3125° (~25 x 25 km²) horizontal resolution over North
644 America as an integrative platform to compare and interpret the ensemble of observations.

645 PM_{2.5} surface observations are fairly homogenous across the Southeast US, reflecting
646 regional coherence in stagnation, mixing, and ventilation. Sulfate and OA account for the bulk of
647 PM_{2.5}. GEOS-Chem simulates sulfate without bias but this requires uncertain consideration of
648 SO₂ oxidation by stabilized Criegee intermediates to account for 30% of sulfate production in the
649 Southeast US. We reproduce the major features of OA observations with a simple
650 parameterization assuming irreversible condensation of low-volatility VOC oxidation products.
651 Marais et al. (2015) show that the default SOA mechanism in GEOS-Chem, based on reversible
652 partitioning of semivolatile products of VOC oxidation (Pye et al., 2010), underestimates
653 isoprene SOA formation by a factor of 3 in the SEAC⁴RS observations. Our OA simulation bias
654 is +14% relative to CSN sites and +66% relative to IMPROVE sites but the IMPROVE data may
655 be too low. OA in the model originates from biogenic isoprene (40%) and monoterpenes (20%),
656 anthropogenic sources (30%) and open fires (10%). Marais et al. (2015) present an improved
657 GEOS-Chem simulation of isoprene SOA in SEAC⁴RS using an aqueous-phase mechanism with
658 irreversible uptake coupled to the gas-phase isoprene oxidation cascade and separating the
659 contributions from the high-NO and low-NO pathways. This mechanism provides in particular a

Daniel Jacob 9/2/2015 3:33 PM
Deleted: The

661 [successful simulation of observations for the OA-formaldehyde relationship and for the](#)
662 [concentration of SOA formed from isoprene epoxides.](#)

663 Aircraft vertical profiles show that 60% of the aerosol column mass is in the mixed layer
664 (ML), 25% is in the convective cloud layer (CCL), and 15% is in the free troposphere (FT). This
665 is well reproduced in GEOS-Chem. OA accounts for 65% of the aerosol column mass in the
666 observations and in the model. The successful simulation of OA vertical profiles argues against a
667 large OA source in the free troposphere other than PBL ventilation. Occasional fire and dust
668 plumes were observed in the free troposphere but have little impact on temporal averages.

669 The extent of neutralization of sulfate aerosol over the Southeast US ($f = [\text{NH}_4^+]/(2[\text{SO}_4^{2-}]$
670 $+ [\text{NO}_3^-])$) is observed to be in the range 0.49-0.68 mol mol⁻¹ for the different data sets, despite an
671 excess of ammonia being present. This is inconsistent with thermodynamic equilibrium and with
672 the observation of a 2003-2013 decline in ammonium aerosol concentrations paralleling that of
673 sulfate. We hypothesize that the departure from equilibrium is correlated with OA, as supported
674 by laboratory findings by Liggio et al. (2011) that organic particle material may impede ammonia
675 uptake by sulfate aerosol. This may have important implications for aerosol hygroscopicity and
676 chemistry.

677 The vertical profile of aerosol light extinction measured from the aircraft follows closely
678 that of aerosol mass. GEOS-Chem has a ~16% low bias in aerosol extinction compared to these
679 observations and simulates correctly the vertical profile. Sulfate accounts for as much of the
680 column light extinction as OA, despite lower mass concentrations. Evaluation of collocated
681 MODIS and MISR AOD retrievals with AERONET shows excellent agreement. GEOS-Chem is
682 16% too low compared to AERONET and 7-28% too low compared to MODIS and MISR,
683 consistent with its bias relative to the aircraft extinction data. We thus find reasonable agreement
684 between AODs measured from space and from the surface, aircraft aerosol extinction and mass
685 profiles, and surface PM_{2.5} measurements, the largest discrepancy being between different
686 measurements of OA.

687 We find that the previously reported summer-to-winter decrease in MODIS AOD data
688 over the Southeast US is driven by a sharp August-to-October transition, in all years. This
689 seasonal transition is well captured by GEOS-Chem where it is caused by declines in both sulfate
690 and OA. Biogenic emissions of isoprene and monoterpenes shut down during this time period due
691 to lower temperatures and leaf senescence, and rapidly declining UV radiation suppresses SO₂
692 oxidation by OH and H₂O₂. The seasonal decline of UV radiation also suppresses the low-NO
693 pathway of isoprene oxidation, which may be associated with larger OA yields than the high-NO
694 pathway.

695 Previous studies have pointed out an apparent inconsistency between the large seasonal
696 variation of AOD measured from space and the much weaker seasonal variation of PM_{2.5}
697 measured at the surface (Goldstein et al., 2009; Ford and Heald, 2013). We find that this can be
698 explained at least in part by the seasonal trend in boundary layer ventilation, offsetting the effect
699 of decreased wintertime PM sources on the surface concentrations. Overall our results show that
700 measured AODs from space are consistent with measurements of PM_{2.5} air quality in the
701 Southeast US. This implies that satellite measurements can reliably be used to infer PM_{2.5} if a
702 good CTM representation of PBL mixing and ventilation is available.

703
704
705
706
707
708
709
710
711
712
713
714
715
716
717
718
719
720
721
722
723
724
725
726
727
728

Daniel Jacob 8/31/2015 10:15 PM

Deleted: largely

730 **Acknowledgements**

731

732 We are grateful to the entire NASA SEAC⁴RS team for their help in the field. We thank
733 Aaron van Donkelaar, Eloise Marais, Loretta Mickley, Randall Martin, Chuck Brock, Ann
734 Dillner, Ralph Kahn, Armin Sorooshian, Tran Nguyen, and Jenny Hand for helpful discussions
735 and Sajeev Philip for assistance with downloading meteorological fields. We also thank Jack
736 Dibb, Bruce Anderson and the LARGE team, Phil Russell, Jens Redemann and the 4STAR team,
737 and Greg Huey for the data shown in the Supplementary Material. This work was funded by the
738 NASA Tropospheric Chemistry Program and by a Department of Energy Office of Science
739 Graduate Fellowship to PSK made possible in part by the American Recovery and Reinvestment
740 Act of 2009, administered by ORISE-ORAU under contract no. DE-AC05-06OR23100. PCJ and
741 JLJ were supported by NASA NNX12AC03G and NSF AGS-1243354/1360834. KF and JL are
742 supported by NASA grant NNH12AT29I from the Upper Atmosphere Research Program,
743 Radiation Sciences Program, and Tropospheric Chemistry Program, and by NOAA base funding.
744 DBM acknowledges support from NSF (Grant #1148951). POW, JDC, JMS, and APT
745 acknowledge support from NASA (NNX12AC06G and NNX14AP46G). We thank the U.S. EPA
746 for providing the 2010 North American emission inventory. The inventory is intended for
747 research purposes and was developed for Phase 2 of the Air Quality Model Evaluation
748 International Initiative (AQMEII) using information from the 2008-based modeling platform as a
749 starting point. A technical document describing the 2008-based 2007v5 modeling platform can be
750 found at epa.gov/ttn/chief/emch/2007v5/2007v5_2020base_EmisMod_TSD_13dec2012.pdf. A
751 report on the 2008 NEI can be found at www.epa.gov/ttn/chief/net/2008report.pdf. GEOS-Chem
752 is managed by the Harvard University Atmospheric Chemistry Modeling Group with support
753 from the NASA Atmospheric Composition Modeling and Analysis Program. The GEOS-FP data
754 used in this study were provided by the Global Modeling and Assimilation Office (GMAO) at
755 NASA Goddard Space Flight Center.

756

757

758

759

760

761

762

763

764 **References**

765

766 Alston, E. J., Sokolik, I. N., and Kalashnikova, O. V.: Characterization of atmospheric aerosol in
767 the US Southeast from ground- and space-based measurements over the past decade,
768 *Atmos. Meas. Tech.*, 5, 1667-1682, doi:10.5194/amt-5-1667-2012, 2012.

769 Attwood, A. R., Washenfelder, R. A., Brock, C. A., Hu, W., Baumann, K., Campuzano-Jost, P.,
770 Day, D. A., Edgerton, E. S., Murphy, D. M., Palm, B. B., McComiskey, A., Wagner, N.
771 L., de Sa, S. S., Ortega, A., Martin, S. T., Jimenez, J. L., and Brown, S. S.: Trends in
772 sulfate and organic aerosol mass in the Southeast U.S.: Impact on aerosol optical depth
773 and radiative forcing, *Geophys. Res. Lett.*, 41, 7701-7709, doi:10.1002/2014GL061669,
774 2014.

775 Baasandorj, M., Millet, D. B., Hu, H., Mitroo, D., and Williams, B. J.: Measuring acetic and
776 formic acid by proton-transfer-reaction mass spectrometry: sensitivity, humidity
777 dependence, and quantifying interferences, *Atmos. Meas. Tech.*, 8, 1303-1321,
778 doi:10.5194/amt-8-1303-2015, 2015.

779 Barsanti, K. C., Carlton, A. G., and Chung, S. H.: Analyzing experimental data and model
780 parameters: implications for predictions of SOA using chemical transport models, *Atmos.*
781 *Chem. Phys.*, 13, 12073-12088, doi:10.5194/acp-13-12073-2013, 2013

782 Blanchard, C. L., Hidy, G. M., Tanenbaum, S., Edgerton, E., Hartsell, B., and Jansen, J.: Carbon
783 in southeastern US aerosol particles: empirical estimates of secondary organic aerosol
784 formation, *Atmos. Environ.*, 42, 6710-6720, doi:10.1016/j.atmosenv.2008.04.011, 2008.

785 Blanchard, C. L., Hidy, G. M., Tanenbaum, S., Edgerton, E. S., and Hartsell, B. E.: The
786 Southeastern Aerosol Research and Characterization (SEARCH) study: Temporal trends
787 in gas and PM concentrations and composition, 1999-2010, *J. Air Waste Manage. Assoc.*,
788 63(3), 247-259, doi:10.1080/10962247.2012.748523, 2013.

789 Boy, M., Mogensen, D., Smolander, S., Zhou, L., Nieminen, T., Paasonen, P., Plass-Dulmer, C.,
790 Sipila, M., Petaja, T., Mauldin, L., Berresheim, H., and Kulmala, M.: Oxidation of SO₂
791 by stabilized Criegee Intermediate (sCI) radicals as a crucial source for atmospheric
792 sulfuric acid concentrations, *Atmos. Chem. Phys.*, 13, 3865-3879, doi:10.5194/acp-13-
793 3865-2013, 2013.

794 Boys, B. L., Martin, R. V., van Donkelaar, A., MacDonell, R. J., Hsu, N. C., Cooper, M. J.,
795 Yantosca, R. M., Lu, Z., Streets, D. G., Zhang, Q., and Wang, S. W.: Fifteen-year global
796 time series of satellite-derived fine particulate matter, *Environ. Sci. Technol.*, 48, 11109-
797 11118, doi:10.1021/es502113p, 2014.

798 Budisulistiorini, S. H., Canagaratna, M. R., Croteau, P. L., Marth, W. J., Baumann, K., Edgerton,
799 E. S., Shaw, S. L., Knipping, E. M., Worsnop, D. R., Jayne, J. T., Gold, A., and Surratt, J.
800 D.: Real-time continuous characterization of secondary organic aerosol derived from
801 isoprene epoxydiols in downtown Atlanta, Georgia, using the Aerodyne Chemical
802 Speciation Monitor, *Environ. Sci. Technol.*, 47, 5686-5694, doi:10.1021/es400023n,
803 2013.

804 Campuzano-Jost, P., Palm, B., Day, D., Hu, W., Ortega, A., Jimenez, J., Liao, J., Froyd, K.,
805 Pollack, I., Peischl, J., Ryerson, T., St. Clair, J., Crounse, J., Wennberg, P., Mikoviny, T.,
806 Wisthaler, A., Ziemba, L., and Anderson, B.: Secondary organic aerosol (SOA) derived
807 from isoprene epoxydiols: Insights into formation, aging, and distribution over the
808 continental US from the DC3 and SEAC4RS campaigns, Abstract A33M-02 presented at
809 2014 Fall Meeting, AGU, San Francisco, Calif., 15-19 Dec, 2014.

810 Canagaratna, M. R., Jayne, J. T., Jimenez, J. L., Allan, J. D., Alfarra, M. R., Zhang, Q., Onasch,
811 T. B., Drewnick, F., Coe, H., Middlebrook, A., Delia, A., Williams, L. R., Trimborn, A.
812 M., Northway, M. J., DeCarlo, P. F., Kolb, C. E., Davidovits, P., and Worsnop, D. R.:
813 Chemical and microphysical characterization of ambient aerosols with the aerodyne
814 aerosol mass spectrometer, *Mass Spectrometry Reviews*, 26(2), 185-222,
815 doi:10.1002/mas.20115, 2007.

816 Canagaratna, M. R., Jimenez, J. L., Kroll, J. H., Chen, Q., Kessler, S. H., Massoli, P., Hildebrandt
817 Ruiz, L., Fortner, E., Williams, L. R., Wilson, K. R., Surratt, J. D., Donahue, N. M.,
818 Jayne, J. T., and Worsnop, D. R.: Elemental ratio measurements of organic compounds
819 using aerosol mass spectrometry: characterization, improved calibration, and
820 implications, *Atmos. Chem. Phys.*, 15, 253-272, doi:10.5194/acp-15-253-2015, 2015.

821 Carlton, A. G., Pinder, R. W., Bhave, P. K., and Pouliot, G. A.: To what extent can biogenic SOA
822 be controlled?, *Environ. Sci. Technol.*, 44, 3376-3380, doi:10.1021/es903506b, 2010.

823 Chan, A. W. H., Chan, M. N., Surratt, J. D., Chhabra, P. S., Loza, C. L., Crounse, J. D., Yee, L.
824 D., Flagan, R. C., Wennberg, P. O., and Seinfeld, J. H.: Role of aldehyde chemistry and
825 NO_x concentrations in secondary organic aerosol formation, *Atmos. Chem. Phys.*, 10,
826 7169-7188, doi:10.5194/acp-10-7169-2010, 2010.

827 Chao, W., Hsieh, J.-T., Chang, C.-H., and Lin, J. J.: Direct kinetic measurement of the reaction of
828 the simplest Criegee intermediate with water vapor, *Science*, 347(6223), 751-754,
829 doi:10.1126/science.1261549, 2015.

830 Chen, G., Ziemba, L. D., Chu, D. A., Thornhill, K. L., Schuster, G. L., Winstead, E. L., Diskin,
831 G. S., Ferrarre, R. A., Burton, S. P., Ismail, S., Kooi, S. A., Omar, A. H., Slusher, D. L.,

832 Kleb, M. M., Reid, J. S., Twohy, C. H., Zhang, H., and Anderson, B. E.: Observations of
833 Saharan dust microphysical and optical properties from the Eastern Atlantic during
834 NAMMA airborne field campaign, *Atmos. Chem. Phys.*, 11, 723-740, doi:10.5194/acp-
835 11-723-2011, 2011.

836 Chin, M., and Jacob, D. J.: Anthropogenic and natural contributions to tropospheric sulfate: A
837 global model analysis, *J. Geophys. Res.*, 101(D13), 18691-18699,
838 doi:10.1029/96JD01222, 1996.

839 Chow, J. C., Watson, J. G., Chen, L.-W. A., Rice, J., and Frank, N. H.: Quantification of PM_{2.5}
840 organic carbon sampling artifacts in US networks, *Atmos. Chem. Phys.*, 10, 5223-5239,
841 doi:10.5194/acp-10-5223-2010, 2010.

842 Crawford, J. H., and Pickering, K. E.: DISCOVER-AQ: Advancing strategies for air quality
843 observations in the next decade, *Environmental Manager*, 4-7, 2014.

844 Crouse, J. D., McKinney, K. A., Kwan, A. J., and Wennberg, P. O.: Measurement of gas-phase
845 hydroperoxides by chemical ionization mass spectrometry, *Anal. Chem.*, 78, 6726-6732,
846 doi:10.1021/ac0604235, 2006.

847 Cubison, M. J., Ortega, A. M., Hayes, P. L., Farmer, D. K., Day, D., Lechner, M. J., Brune, W.
848 H., Apel, E., Diskin, G. S., Fisher, J. A., Fuelberg, H. E., Hecobian, A., Knapp, D. J.,
849 Mikoviny, T., Riemer, D., Sachse, G. W., Sessions, W., Weber, R. J., Weinheimer, A. J.,
850 Wisthaler, A., and Jimenez, J. L.: Effects of aging on organic aerosol from open biomass
851 burning smoke in aircraft and laboratory studies, *Atmos. Chem. Phys.*, 11, 12049-12064,
852 doi:10.5194/acp-11-12049-2011, 2011.

853 Darmenov, A., and da Silva, A.: The Quick Fire Emissions Dataset (QFED) – Documentation of
854 versions 2.1, 2.2, and 2.4, NASA Technical Report Series of Global Modeling and Data
855 Assimilation, NASA TM-2013-104606, 32, 183 pp, 2013.

856 de Gouw, J. A., and Jimenez, J. L.: Organic aerosols in the Earth's atmosphere, *Environ. Sci.*
857 *Technol.*, 43, 7614-7618, doi:10.1021/es9006004, 2009.

858 Dibb, J. E., Talbot, R. W., Scheuer, E. M., Seid, G., Avery, M. A., and Singh, H. B.: Aerosol
859 chemical composition in Asian continental outflow during the TRACE-P campaign:
860 comparison with PEM-West B, *J. Geophys. Res.*, 108, 8815, doi:10.1029/2002JD003111,
861 D21, 2003.

862 Dillner, A. M., Phuah, C. H., and Turner, J. R.: Effects of post-sampling conditions on ambient
863 carbon aerosol filter measurements, *Atmos. Environ.*, 43, 5937-5943,
864 doi:10.1016/j.atmosenv.2009.08.009, 2009.

865 Diner, D. J., Braswell, B. H., Davies, R., Gobron, N., Hu, J., Jin, Y., Kahn, R. A., Knyazikhin,
866 Loeb, N., Muller, J.-P., Nolin, A. W., Pinty, B., Schaaf, C. B., Seiz, G., and Stroeve, J.:
867 The value of multiangle measurements for retrieving structurally and radiatively
868 consistent properties of clouds, aerosols, and surfaces, *Remote Sens. Environ.*, *97*, 495-
869 518, doi:10.1016/j.rse.2005.06.006, 2005.

870 Docherty, K. S., Stone, E. A., Ulbrich, I. M., DeCarlo, P. F., Snyder, D. C., Schauer, J. J., Peltier,
871 R. E., Weber, R. J., Murphy, S. M., Seinfeld, J. H., Grover, B. D., Eatough, D. J., and
872 Jimenez, J. L.: Apportionment of primary and secondary organic aerosols in Southern
873 California during the 2005 Study of Organic Aerosols in Riverside (SOAR-1), *Environ.*
874 *Sci. Technol.*, *42*, 7655-7662, doi:10.1021/es8008166, 2008.

875 Donahue, N. M., Robinson, A. L., Stanier, C. O., and Pandis, S. N.: Coupled partitioning,
876 dilution, and chemical aging of semivolatile organics, *Environ. Sci. Technol.*, *40*, 2635-
877 2643, doi:10.1021/es052297c, 2006.

878 Drury, E., Jacob, D. J., Spurr, R. J. D., Wang, J., Shinzuka, Y., Anderson, B. E., Clarke, A. D.,
879 Dibb, J., McNaughton, C., and Weber, R.: Synthesis of satellite (MODIS), aircraft
880 (ICARTT), and surface (IMPROVE, EPA-AQS, AERONET) aerosol observations over
881 eastern North America to improve MODIS aerosol retrievals and constrain surface
882 aerosol concentrations and sources, *J. Geophys. Res.*, *115*, D14204,
883 doi:10.1029/2009JD012629, 2010.

884 Eddingsaas, N. C., VanderVelde, D. G., and Wennberg, P. O.: Kinetics and products of the acid-
885 catalyzed ring-opening of atmospherically relevant butyl epoxy alcohols, *J. Phys. Chem.*
886 *A*, *114*, 8106-8113, doi:10.1021/jp103907c, 2010.

887 Edgerton, E. S., Hartsell, B. E., Saylor, R. D., Jansen, J. J., Hansen, D. A., and Hidy, G. M.: The
888 Southeastern Aerosol Research and Characterization Study: Part II. Filter-based
889 measurements of fine and coarse particulate matter mass and composition, *J. Air &*
890 *Waste Manage. Assoc.*, *52*, 1527-1542, doi:10.1080/10473289.2005.10464744, 2005.

891 Edgerton, E. S., et al.: First look at ¹⁴C data during the Centreville, AL SOAS campaign,
892 presented at the SAS Data Workshop, Boulder, Co., 31 Mar. – 2 Apr, 2014.

893 EPA.: Particulate matter (PM_{2.5}) speciation guidance, Final draft, Edition 1, October 7, 1999. U.S.
894 Environmental Protection Agency, Monitoring and Quality Assurance Group, Emissions,
895 Monitoring, and Analysis Division, Office of Air Quality Planning and Standards,
896 Research Triangle Park, NC. [http://www.epa.gov/ttn/amtic/files/ambient/
897 pm25/spec/specfinl.pdf](http://www.epa.gov/ttn/amtic/files/ambient/pm25/spec/specfinl.pdf), 1999.

898 Ervens, B., Turpin, B. J., and Weber, R. J.: Secondary organic aerosol formation in cloud droplets

899 and aqueous particles (aqSOA): a review of laboratory, field and model studies, *Atmos.*
900 *Chem. Phys.*, 11, 11069-11102, doi:10.5194/acp-11-11069-2011, 2011.

901 Fairlie, T. D., Jacob, D. J., and Park, R. J.: The impact of transpacific transport of mineral dust in
902 the United States, *Atmos. Environ.*, 41, 1251-1266, doi:10.1016/j.atmosenv.2006.09.048,
903 2007.

904 Fischer, E. V., Jacob, D. J., Yantosca, R. M., Sulprizio, M. P., Millet, D. B., Mao, J., Paulot, F.,
905 Singh, H. B., Roiger, A., Ries, L., Talbot, R. W., Dzepina, K., and Pandey Deolal, S.:
906 Atmospheric peroxyacetyl nitrate (PAN): a global budget and source attribution, *Atmos.*
907 *Chem. Phys.*, 14, 2679-2698, doi:10.5194/acp-14-2679-2014, 2014.

908 Fisher, J. A., Jacob, D., Travis, K., Cohen, R., Fried, A., Hanisco, T., Mao, J., Wennberg, P.,
909 Crounse, J., St. Clair, J., Teng, A., Wisthaler, A., Mikoviny, T., Jimenez, J., Campuzano-
910 Jost, P., Kim, P., Marais, E., Paulot, F., Yu, K., Zhu, L., Yantosca, R., and Sulprizio, M.:
911 Isoprene nitrate chemistry in the Southeast US: Constraints from GEOS-Chem and
912 SEAC⁴RS, presented at the SEAC⁴RS Science Team Meeting, Pasadena, Calif., 28 Apr –
913 1 May, 2015.

914 Ford, B., and Heald, C. L.: Aerosol loading in the Southeastern United States: reconciling surface
915 and satellite observations, *Atmos. Chem. Phys.*, 13, 9269-9283, doi:10.5194/acp-13-
916 9269-2013, 2013.

917 Fountoukis, C., and Nenes, A.: ISORROPIA II: a computationally efficient thermodynamic
918 equilibrium model for K^+ - Ca^{2+} - Mg^{2+} - NH_4^+ - Na^+ - SO_4^{2-} - NO_3^- - Cl^- - H_2O aerosols, *Atmos.*
919 *Chem. Phys.*, 7, 4639-4659, doi:10.5194/acp-7-4639-2007, 2007.

920 Froyd, K. D., Murphy, S. M., Murphy, D. M., de Gouw, J. A., Eddingsaas, N. C., and Wennberg
921 P. O.: Contribution of isoprene-derived organosulfates to free tropospheric aerosol mass,
922 *Proc. Natl. Acad. Sci.*, 107(50), 21360-21365, doi:10.1073/pnas.1012561107, 2010.

923 Fu, T. M., Jacob, D. J., and Heald, C. L.: Aqueous-phase reactive uptake of dicarbonyls as a
924 source of organic aerosol over eastern North America, *Atmos. Environ.*, 43, 1814-1822,
925 doi: 10.1016/j.atmosenv.2008.12.029, 2009.

926 Goldstein, A. H., Koven, C. D., Heald, C. L., and Fung, I. Y.: Biogenic carbon and anthropogenic
927 pollutants combine to form a cooling haze over the southeastern United States, *Proc.*
928 *Natl. Acad. Sci.*, 106(22), 8835-8840, doi:10.1073/pnas.0904128106, 2009.

929 Guenther, A. B., Jiang, X., Heald, C. L., Sakulyanontvittaya, T., Duhl, T., Emmons, L. K., and
930 Wang, X.: The Model of Emissions of Gases and Aerosols from Nature version 2.1
931 (MEGAN2.1): an extended and updated framework for modeling biogenic emissions,
932 *Geosci. Model Dev.*, 5, 1471-1492, doi:10.5194/gmd-5-1471-2012, 2012.

933 Hair, J. W., Hostetler, C. A., Cook, A. L., Harper, D. B., Ferrare, R. A., Mack, T. L., Welch, W.,
934 Izquierdo, L. R., and Hovis, F. E.: Airborne High Spectral Resolution Lidar for profiling
935 aerosol optical properties, *Appl. Optics*, 47, 6734-6752, doi:10.1364/AO.47.006734,
936 2008.

937 Hand, J. L., Schichtel, B. A., Pitchford, M., Malm, W. C., and Frank, N. H.: Seasonal
938 composition of remote and urban fine particulate matter in the United States, *J. Geophys.*
939 *Res.*, 117, D05209, doi:10.1029/2011JD017122, 2012a.

940 Hand, J. L., Schichtel, B. A., Malm, W. C., and Pitchford, M. L.: Particulate sulfate ion
941 concentration and SO₂ emission trends in the United States from the early 1990s through
942 2010, *Atmos. Chem. Phys.*, 12, 10353-10365, doi:10.5194/acp-12-10353-2012, 2012b.

943 Hayes, P. L., Carlton, A. G., Baker, K. R., Ahmadov, R., Washenfelder, R. A., Alvarez, S.
944 Rappengluck, B., Gilman, J. B., Kuster, W. C., de Gouw, J. A., Zotter, P., Prevot, A. S.
945 H., Szidat, S., Kleindienst, T. E., Offenberg, J. H., and Jimenez, J. L.: Modeling the
946 formation and aging of secondary organic aerosols in Los Angeles during CalNex 2010,
947 *Atmos. Chem. Phys. Discuss*, 14, 32325-32391, doi:10.5194/acpd-14-32325-2014, 2014.

948 Heald, C. L., Jacob, D. J., Turquety, S., Hudman, R. C., Weber, R. J., Sullivan, A. P., Peltier, R.
949 E., Atlas, E. L., de Gouw, J. A., Warneke, C., Holloway, J. S., Neuman, J. A., Flocke, F.
950 M., and Seinfeld, J. H.: Concentrations and sources of organic carbon aerosols in the free
951 troposphere over North America, *J. Geophys. Res.*, 111, D23S47,
952 doi:10.1029/2006JD007705, 2006a.

953 Heald, C. L., Jacob, D. J., Park, R. J., Alexander, B., Fairlie, T. D., Yantosca, R. M., and Chu, D.
954 A.: Transpacific transport of Asian anthropogenic aerosols and its impact on surface air
955 quality in the United States, *J. Geophys. Res.*, 111, D14310, doi:10.1029/2005JD006847,
956 2006b.

957 Heald, C. L., Coe, H., Jimenez, J. L., Weber, R. J., Bahreini, R., Middlebrook, A. M., Russell, L.
958 M., Jolleys, M., Fu, T.-M., Allan, J. D., Bower, K. N., Capes, G., Crosier, J., Morgan, W.
959 T., Robinson, N. H., Williams, P. I., Cubison, M. J., DeCarlo, P. F., and Dunlea, E. J.:
960 Exploring the vertical profile of atmospheric organic aerosol: comparing 17 aircraft field
961 campaigns with a global model, *Atmos. Chem. Phys.*, 11, 12673-12696, doi:10.5194/acp-
962 11-12673-2011, 2011.

963 Heald, C. L., Collett Jr., J. L., Lee, T., Benedict, K. B., Schwandner, F. M., Li, Y., Clarisse, L.,
964 Hurtmans, D. R., Van Damme, M., Clerbaux, C., Coheur, P.-F., Philip, S., Martin, R. V.,
965 and Pye, H. O. T.: Atmospheric ammonia and particulate inorganic nitrogen over the

966 United States, *Atmos. Chem. Phys.*, 12, 10295-10312, doi:10.5194/acp-12-10295-2012,
967 2012.

968 Henze, D. K., and Seinfeld, J. H.: Global secondary organic aerosol from isoprene oxidation,
969 *Geophys. Res. Lett.*, 33, L09812, doi:10.1029/2006GL025976, 2006.

970 Hermansson, E., Roldin, P., Rusanen, A., Mogensen, D., Kivekas, N., Vaananen, R., Boy, M.,
971 and Swietlicki, E.: Biogenic SOA formation through gas-phase oxidation and gas-to-
972 particle partitioning – a comparison between process models of varying complexity,
973 *Atmos. Chem. Phys.*, 14, 11853-11869, doi:10.5194/acp-14-11853-2014, 2014.

974 Hidy, G. M., Blanchard, C. L., Baumann, K., Edgerton, E., Tanenbaum, S., Shaw, S., Knipping,
975 E., Tombach, I., Jansen, J., and Walters, J.: Chemical climatology of the southeastern
976 United States, 1999-2013, *Atmos. Chem. Phys.*, 14, 11893-11914, doi:10.5194/acp-14-
977 11893-2014, 2014.

978 Hodzic, A., and Jimenez, J. L.: Modeling anthropogenically controlled secondary organic
979 aerosols in a megacity: a simplified framework for global and climate models, *Geosci.*
980 *Model Dev.*, 4, 901-917, doi:10.5194/gmd-4-901-2011, 2011.

981 Holben, B. N., Eck, T. F., Slutsker, I., Tanre, D., Buis, J. P., Setzer, A., Vermote, E., Reagan, J.
982 A., Kaufman, Y. J., Nakajima, T., Lavenu, F., Jankowiak, I., and Smirnov, A.:
983 AERONET – A federated instrument network and data archive for aerosol
984 characterization, *Remote Sens. Environ.*, 66, 1-16, doi:10.1016/S0034-4257(98)00031-5.,
985 1998.

986 Hoyle, C., Boy, M., Donahue, N. M., Fry, J. L., Glasius, M., Guenther, A., Hallar, A. G., Huff
987 Hartz, K., Petters, M. D., Petaja, T., Rosenoern, T., and Sullivan, A. P.: A review of the
988 anthropogenic influence on biogenic secondary organic aerosol, *Atmos. Chem. Phys.*, 11,
989 321-343, doi:10.5194/acp-11-321-2011, 2011.

990 Hu, W., Campuzano-Jost, P., Palm, B. B., Day, D. A., Ortega, A. M., Hayes, P. L., Krechmer, J.
991 E., Chen, Q., Kuwata, M., Liu, Y. J., de Sa, S. S., Martin, S. T., Hu, M., Budisulistiorini,
992 S. H., Riva, M., Surratt, J. D., St. Clair, J. M., Isaacman-Van Wertz, G., Yee, L. D.,
993 Goldstein, A. H., Carbone, S., Artaxo, P., de Gouw, J. A., Koss, A., Wisthaler, A.,
994 Mikoviny, T., Karl, T., Kaser, L., Jud, W., Hansel, A., Docherty, K. S., Robinson, N. H.,
995 Coe, H., Allan, J. D., Canagaratna, M. R., Paulot, F., and Jimenez, J. L.: Characterization
996 of a real-time tracer for isoprene epoxydiols-derived secondary organic aerosol (IEPOX-
997 SOA) from aerosol mass spectrometer measurements, *Atmos. Chem. Phys. Discuss.*, 15,
998 11223-11276, doi:10.5194/acpd-15-11223-2015, 2015.

999 Hu, X., Walker, L. A., Lyapustin, A., Wang, Y., and Liu, Y.: 10-year spatial and temporal trends
1000 of PM_{2.5} concentrations in the southeastern US estimated using high-resolution satellite
1001 data, *Atmos. Chem. Phys.*, 14, 6301-6314, doi:10.5194/acp-14-6301-2014, 2014.

1002 Hu, L., Millet, D. B., Baasandorj, M., Griffis, T. J., Turner, P., Helmig, D., Curtis, A. J., and
1003 Hueber, J.: Isoprene emissions and impacts over an ecological transition region in the US
1004 Upper Midwest inferred from tall tower measurements, *J. Geophys. Res.*, in press,
1005 doi:10.1002/2014JD022732, 2015.

1006 Hudman, R. C., Moore, N. E., Mebust, A. K., Martin, R. V., Russell, A. R., Valin, L. C. and
1007 Cohen, R. C.: Steps towards a mechanistic model for global soil nitric oxide emissions:
1008 implementation and space-based constraints, *Atmos. Chem. Phys.*, 12, 7770 – 7795,
1009 doi:10.5194/acp-12-7779-2012, 2012.

1010 Jacob, D. J., Horowitz, L. W., Munger, J. W., Heikes, B. G., Dickerson, R. R., Artz, R. S. and
1011 Keene, W. C.: Seasonal transition from NO_x- to hydrocarbon-limited conditions for
1012 ozone production over the eastern United States in September, *J. Geophys. Res.*,
1013 100(D5), 9315-9324, doi:10.1029/94JD03125, 1995.

1014 Jaegle, L., Quinn, P. K., Bates, T. S., Alexander, B., and Lin, J.-T.: Global distribution of sea salt
1015 aerosols: new constraints from in situ and remote sensing observations, *Atmos. Chem.*
1016 *Phys.*, 11, 3137-3157, doi:10.5194/acp-11-3137-2011, 2011.

1017 Jenkin, M. E., Saunders, S. M., and Pilling, M. J.: The tropospheric degradation of volatile
1018 organic compounds: A protocol for mechanism development, *Atmos. Environ.*, 31, 81-
1019 104, doi:10.1016/s1352-2310(96)00105-7, 1997.

1020 Jimenez, J. L., Canagaratna, M. R., Donahue, N. M., Prevot, A. S. H., Zhang, Q., Kroll, J. H.,
1021 DeCarlo, P. F., Allan, J. D., Coe, H., Ng, N. L., Aiken, A. C., Docherty, K. S., Ulbrich, I.
1022 M., Grieshop, A. P., Robinson, A. L., Duplissy, J., Smith, J. D., Wilson, K. R., Lanz, V.
1023 A., Hueglin, C., Sun, Y. L., Tian, J., Laak-sonen, A., Raatikainen, T., Rautiainen, J.,
1024 Vaattovaara, P., Ehn, M., Kulmala, M., Tomlinson, J. M., Collins, D. R., Cubison, M. J.,
1025 Dunlea, E. J., Huffman, J. A., Onasch, T. B., Alfarra, M. R., Williams, P. I., Bower, K.,
1026 Kondo, Y., Schneider, J., Drewnick, F., Borrmann, S., Weimer, S., Demerjian, K.,
1027 Salcedo, D., Cottrell, L., Griffin, R., Takami, A., Miyoshi, T., Hatakeyama, S.,
1028 Shimono, A., Sun, J. Y., Zhang, Y. M., Dzepina, K., Kimmel, J. R., Sueper, D., Jayne, J.
1029 T., Herndon, S. C., Trimborn, A. M., Williams, L. R., Wood, E. C., Middlebrook, A. M.,
1030 Kolb, C. E., Baltensperger, U., and Worsnop, D. R.: Evolution of organic aerosols in the
1031 Atmosphere, *Science*, 326, 1525–1529, doi:10.1126/science.1180353, 2009.

1032 Jolleys, M. D., Coe, H., McFiggans, G., Capes, G., Allan, J. D., Crosier, J., Williams, P. I., Allen,
1033 G., Bower, K. N., Jimenez, J. L., Russell, L. M., Grutter, M., and Baumgardner, D.:
1034 Characterizing the aging of biomass burning organic aerosol by use of mixing ratios: a
1035 meta-analysis of four regions, *Environ. Sci. Technol.*, 46, 13093-13102,
1036 doi:10.1021/es302386v, 2012.

1037 Kim, P. S., Jacob, D. J., Liu, X., Warner, J. X., Yang, K., Chance, K., Thouret, V., and Nedelec,
1038 P.: Global ozone-CO correlations from OMI and AIRS: constraints on tropospheric ozone
1039 sources, *Atmos. Chem. Phys.*, 13, 9321-9335, doi:10.5194/acp-13-9321-2013, 2013.

1040 Kleindienst, T. E., Jaoui, M., Lewandowski, M., Offenber, J. H., Lewis, C. W., Bhave, P. V.,
1041 and Edney, E. O.: Estimates of the contributions of biogenic and anthropogenic
1042 hydrocarbons to secondary organic aerosol at a southeastern US location, *Atmos.*
1043 *Environ.*, 41, 8288-8300, doi:10.1016/j.atmosenv.2007.06.045, 2007.

1044 Kleinman, L. I.: Seasonal dependence of boundary layer peroxide concentration: The low and
1045 high NO_x regimes, *J. Geophys. Res.*, 96(D11), 20721 – 20733, doi:10.1029/91JD02040,
1046 1991.

1047 Koepke P., Hess, M., Schult, I., and Shettle, E. P.: Global Aerosol Data Set, Max-Planck-Institut
1048 fur Meteorologie, Hamburg, 1997.

1049 Kroll, J. H., Ng, N. L., Murphy, S. M., Flagan, R. C., and Seinfeld, J. H.: Secondary organic
1050 aerosol formation from isoprene photooxidation under high-NO_x conditions, *Geophys.*
1051 *Res. Lett.*, 32, L18808, doi:10.1029/2005GL023637, 2005.

1052 Kroll, J. H., Ng, N. L., Murphy, S. M., Flagan, R. C., and Seinfeld, J. H.: Secondary organic
1053 aerosol formation from isoprene photooxidation, *Environ. Sci. Technol.*, 40, 1869-1877,
1054 doi:10.1021/es0524301, 2006.

1055 Langridge, J. M., Richardson, M. S., Lack, D., Law, D., and Murphy, D. M.: Aircraft instrument
1056 for comprehensive characterization of aerosol optical properties, Part I: Wavelength-
1057 dependent optical extinction and its relative humidity dependence measured using cavity
1058 ringdown spectroscopy, *Aerosol Sci. Technol.*, 45(11), 1305:1318,
1059 doi:10.1080/02786826.2011.592745, 2011.

1060 Leibensperger, E. M., Mickley, L. J., Jacob, D. J., Chen, W.-T., Seinfeld, J. H., Nenes, A.,
1061 Adams, P. J., Streets, D. G., Kumar, N., and Rind, D.: Climatic effects of 1950-2050
1062 changes in US anthropogenic aerosols – Part I: Aerosol trends and radiative forcing,
1063 *Atmos. Chem. Phys.*, 12, 3333-3348, doi:10.5194/acp-12-3333-2012, 2012a.

1064 Leibensperger, E. M., Mickley, L. J., Jacob, D. J., Chen, W.-T., Seinfeld, J. H., Nenes, A.,
1065 Adams, P. J., Streets, D. G., Kumar, N., and Rind, D.: Climatic effects of 1950-2050

1066 changes in US anthropogenic aerosols – Part 2: Climate response, *Atmos. Chem. Phys.*,
1067 12, 3349-3362, doi:10.5194/acp-12-3349-2012, 2012b.

1068 Levy, R. C., Mattoo, S., Munchak, L. A., Remer, L. A., Sayer, A. M., Patadia, F., and Hsu, N. C.:
1069 The Collection 6 MODIS aerosol products over land and ocean, *Atmos. Meas. Tech.*, 6,
1070 2989-3034, doi:10.5194/amt-6-2989-2013, 2013.

1071 Li, J., Ying, Q., Yi, B., and Yang, P.: Role of stabilized Criegee Intermediates in the formation of
1072 atmospheric sulfate in eastern United States, *Atmos. Environ.*, 79, 442-447,
1073 doi:10.1016/j.atmosenv.2013.06.048, 2013.

1074 Liao, J., Froyd, K. D., Murphy, D. M., Keutsch, F. N., Yu, G., Wennberg, P. O., St. Clair, J. M.,
1075 Crounse, J. D., Wisthaler, A., Mikoviny, T., Jimenez, J. L., Campuzano-Jost, P., Day, D.
1076 A., Hu, W., Ryerson, T. B., Pollack, I. B., Peischl, J., Anderson, B. E., Ziemba, L. D.,
1077 Blake, D. R., Meinardi, S., and Diskin, G.: Airborne measurements of organosulfates
1078 over the continental U. S., *J. Geophys. Res.*, 120, doi:10.1002/2014JD022378, 2015.

1079 Liggio, J., Li, S.-M., Vlasenko, A., Stroud, C., and Makar, P.: Depression of ammonium uptake to
1080 sulfuric acid aerosols by competing uptake of ambient organic gases, *Environ. Sci.*
1081 *Technol.*, 45, 2790-2796, doi:10.1021/es103801g, 2011.

1082 Lim, H.-J., and Turpin, B. J.: Origins of primary and secondary organic aerosol in Atlanta: results
1083 of time-resolved measurements during the Atlanta Supersite Experiment, *Environ. Sci.*
1084 *Technol.*, 36, 4489-4496, doi:10.1021/es0206487, 2002.

1085 Lin, J.-T., and McElroy, M. B.: Impacts of boundary layer mixing on pollutant vertical profiles in
1086 the lower troposphere: Implications to satellite remote sensing, *Atmos. Environ.*, 44,
1087 1726-739, doi:10.1016/j.atmosenv.2010.02.009, 2010.

1088 Liu, D., Wang, Z., Liu, Z., Winker, D., and Trepte, C.: A height resolved global view of dust
1089 aerosols from the first year CALIPSO lidar measurements, *J. Geophys. Res.*, 113,
1090 D16214, doi:10.1029/2007JD009776, 2008.

1091 Liu, H., Jacob, D. J., Bey, I., and Yantosca, R. M.: Constraints from ^{210}Pb and ^7Be on wet
1092 deposition and transport in a global three-dimensional chemical tracer model driven by
1093 assimilated meteorological fields, *J. Geophys. Res.*, 106(D11), 12109–12128,
1094 doi:10.1029/2000JD900839, 2001.

1095 Liu Y., Park, R. J., Jacob, D. J., Li, Q., Kilaru, V., and Sarnat, J. A.: Mapping annual mean
1096 ground-level $\text{PM}_{2.5}$ concentrations using Multiangle Imaging Spectroradiometer aerosol
1097 optical thickness over the contiguous United States, *J. Geophys. Res.*, 109, D22206,
1098 doi:10.1029/2004JD005025, 2004.

1099 Mao, J., Paulot, F., Jacob, D. J., Cohen, R. C., Crouse, J. D., Wennberg, P. O., Keller, C. A.,
1100 Hudman, R. C., Barkley, M. P., and Horowitz, L. W.: Ozone and organic nitrates over the
1101 eastern United States: Sensitivity to isoprene chemistry, *J. Geophys. Res. Atmos.*, 118,
1102 11256-11268, doi:10.1002/jgrd/50817, 2013.

1103 Malm, W. C., Sisler, J. F., Huffman, D., Eldred, R. A., and Cahill, T. A.: Spatial and seasonal
1104 trends in particle concentration and optical extinction in the United States, *J. Geophys.*
1105 *Res.*, 99(D1), 1347-1370, doi:10.1029/93JD02916, 1994.

1106 Marais, E., et al.: A mechanistic model of isoprene aerosol formation for improved understanding
1107 of organic aerosol composition, presented at the SEAC⁴RS Science Team Meeting,
1108 Pasadena, Calif., 28 Apr – 1 May, 2015.

1109 Martin, R. V., Jacob, D. J., Yantosca, R. M., Chin, M., and Ginoux, P.: Global and regional
1110 decreases in tropospheric oxidants from photochemical effects of aerosols, *J. Geophys.*
1111 *Res.*, 108, 4097, doi:10.1029/2002JD002622, 2003.

1112 Martin, S. T., Hung, H.-H., Park, R. J., Jacob, D. J., Spurr, R. J. D., Chance, K. V., and Chin, M.:
1113 Effects of the physical state of tropospheric ammonium-sulfate-nitrate particles on global
1114 aerosol direct radiative forcing, *Atmos. Chem. Phys.*, 4, 183-214, doi:10.5194/acp-4-183-
1115 2004, 2004.

1116 Mauldin III, R. L., Berndt, T., Sipila, M., Paasonen, P., Petaja, T., Kim, S., Kurten, T., Stratmann,
1117 F., Kerminen, V.-M., and Kulmala, M.: A new atmospherically relevant oxidant of
1118 sulphur dioxide, *Nature*, 488, 193-196, doi:10.1038/nature11278, 2012.

1119 McKeen, S., Chung, S. H., Wilczak, J., Grell, G., Djalalova, I., Peckham, S., Gong, W., Bouchet,
1120 V., Moffet, R., Tang, Y., Carmichael, G. R., Mathur, R., and Yu, S.: Evaluation of
1121 several PM_{2.5} forecast models using data collected during the ICARTT/NEAQS 2004
1122 field study, *J. Geophys. Res.*, 112, D10S20, doi:10.1029/2006JD007608, 2007.

1123 McNeill, V. F., Woo, J. L., Kim, D. D., Schwier, A. N., Wannell, N. J., Sumner, A. J., and
1124 Barakat, J. M.: Aqueous-phase secondary organic aerosol and organosulfate formation in
1125 atmospheric aerosols: a modeling study, *Environ. Sci. Technol.*, 46, 8075-8081,
1126 doi:10.1021/es3002986, 2012.

1127 Millet, D. B., Baasandorj, M., Farmer, D. K., Thornton, J. A., Baumann, K., Brophy, P.,
1128 Chaliyakunnel, S., de Gouw, J. A., Graus, M., Hu, L., Koss, A., Lee, B. H., Lopez-
1129 Hilfiker, F. D., Neuman, J. A., Paulot, F., Peischl, J., Pollack, I. B., Ryerson, T. B.,
1130 Warneke, C., Williams, B. J., and Xu, J.: A large and ubiquitous source of atmospheric
1131 formic acid, *Atmos. Chem. Phys. Discuss.*, 15, 4537-4599, doi:10.5194/acpd-15-4537-
1132 2015, 2015.

1133 Murphy, B. N., Donahue, N. M., Fountoukis, C., Dall'Osto, M., O'Dowd, C., Kiendler-Scharr,
1134 A., and Pandis, S. N.: Functionalization and fragmentation during ambient organic
1135 aerosol aging: application of the 2-D volatility basis set to field studies, *Atmos. Chem.*
1136 *Phys.*, 12, 10797-10816, doi:10.5194/acp-12-10797-2012, 2012.

1137 Murphy, D. M., Cziczo, D. J., Froyd, K. D., Hudson, P. K., Matthew, B. M., Middlebrook, A. M.,
1138 Peltier, R. E., Sullivan, A., Thomson, D. S., and Weber, R. J.: Single-particle mass
1139 spectrometry of tropospheric aerosol particles, *J. Geophys. Res.*, 111, D23S32,
1140 doi:10.1029/2006JD007340, 2006.

1141 NADP: National Atmospheric Deposition Program Animated Maps, Available at:
1142 <http://nadp.sws.uiuc.edu/data/animaps.aspx>, Accessed: March 7, 2015, 2015.

1143 Newland, M. J., Rickard, A. R., Alam, M. S., Vereecken, L., Munoz, A., Rodenas, M., and Bloss,
1144 W. J.: Kinetics of stabilised Criegee intermediates derive from alkene ozonolysis:
1145 reactions with SO₂, H₂O and decomposition under boundary layer conditions, *Phys.*
1146 *Chem. Chem. Phys.*, 17, 4076-4088, doi:10.1039/c4cp04186k, 2014.

1147 NOAA National Climatic Data Center: State of the Climate: Wildfires for Annual 2011,
1148 published online December 2011, retrieved on March 26, 2015 from
1149 <http://www.ncdc.noaa.gov/sotc/fire/2011/13>, 2011.

1150 Pankow, J. F.: An absorption model of gas/particle partitioning of organic compounds in the
1151 atmosphere, *Atmos. Environ.*, 28, 185-188, doi:10.1016/1352-2310(94)90093-0, 1994.

1152 Park, R. J., Jacob, D. J., Chin, M., and Martin, R. V.: Sources of carbonaceous aerosols over the
1153 United States and implications for natural visibility, *J. Geophys. Res.*, 108(D12), 4355,
1154 doi:10.1029/2002JD003190, 2003.

1155 Park, R. J., Jacob, D. J., Field, B. D., Yantosca, R. M., and Chin, M.: Natural and transboundary
1156 pollution influences on sulfate-nitrate-ammonium aerosols in the United States:
1157 Implications for policy, *J. Geophys. Res.*, 109, D15204, doi:10.1029/2003JD004473,
1158 2004.

1159 Park, R. J., Jacob, D. J., Kumar, N., and Yantosca, R. M.: Regional visibility statistics in the
1160 United States: Natural and transboundary pollution influences, and implications for the
1161 Regional Haze Rule, *Atmos. Environ.*, 40, 5405-5423,
1162 doi:10.1016/j.atmosenv.2006.04.059, 2006.

1163 Park, R. J., Jacob, D. J., and Logan, J. A.: Fire and biofuel contributions to annual mean aerosol
1164 mass concentrations in the United States, *Atmos. Environ.*, 41, 7389-7400,
1165 doi:10.1016/j.atmosenv.2007.05.061, 2007.

1166 Paulot, F., Jacob, D. J., Pinder, R. W., Bash, J. O., Travis, K., and Henze, D. K.: Ammonia
1167 emissions in the United States, European Union, and China derived by high-resolution
1168 inversion of ammonium wet deposition data: Interpretation with a new agricultural
1169 emissions inventory (MASAGE_NH3), *J. Geophys. Res. Atmos.*, 119, 4343-4364,
1170 doi:10.1002/2013JD021130, 2014.

1171 Peterson, D. A., Hyer, E. J., Campbell, J. R., Fromm, M. D., Hair, J. W., Butler, C. F., and Fenn,
1172 M. A.: The 2013 Rim Fire: Implications for predicting extreme fire spread,
1173 pyroconvection, and smoke emissions, *Bull. Amer. Meteor. Soc.*, doi:10.1175/BAMS-D-
1174 14-00060.1, 2015.

1175 Pfister, L., Rosenlof, K., Ueyama, R., and Heath, N.: A meteorological overview of the SEAC⁴RS
1176 mission, presented at the SEAC⁴RS Science Team Meeting, Pasadena, Calif., 28 Apr – 1
1177 May, 2015.

1178 Pierce, J. R., Evans, M. J., Scott, C. E., D' Andrea, S. D., Farmer, D. K., Swietlicki, E., and
1179 Spracklen, D. V.: Weak global sensitivity of cloud condensation nuclei and aerosol
1180 indirect effect to Criegee + SO₂ chemistry, *Atmos. Chem. Phys.*, 13, 3163-3176,
1181 doi:10.5194/acp-13-3163-2013, 2013.

1182 Pye, H. O. T., Liao, H., Wu, S., Mickleby, L. J., Jacob, D. J., Henze, D. K., and Seinfeld, J. H.:
1183 Effect of changes in climate and emissions on future sulfate-nitrate-ammonium aerosol
1184 levels in the United States, *J. Geophys. Res.*, 114, D01205, doi:10.1029/2008JD010701,
1185 2009.

1186 Pye, H. O. T., Chan, A. W. H., Barkley, M. P., and Seinfeld, J. H.: Global modeling of organic
1187 aerosol: the importance of reactive nitrogen (NO_x and NO₃), *Atmos. Chem. Phys.*, 10,
1188 11261-11276, doi:10.5194/acp-10-11261-2010, 2010.

1189 Remer, L. A., Kaufman, Y. J., Tanre, D., Mattoo, S., Chu, D. A., Martins, J. V., Li, R.-R., Ichoku,
1190 C., Levy, R. C., Kleidman, R. G., Eck, T. F., Vermote, E., and Holben, B. N.: The
1191 MODIS aerosol algorithm, products, and validation, *J. Atmos. Sci.*, 62, 947-973,
1192 doi:10.1175/jas3385.1, 2005.

1193 Russell, A. R., Valin, L. C., and Cohen, R. C.: Trends in OMI NO₂ observations over the United
1194 States: effects of emission control technology and the economic recession, *Atmos. Chem.*
1195 *Phys.*, 12, 12197-12209, doi:10.5194/acp-12-12197-2012, 2012.

1196 Saide, P. E., Peterson, D., da Silva, A., Anderson, B., Ziemba, L. D., Diskin, G., Sachse, G., Hair,
1197 J., Butler, C., Fenn, M., Jimenez, J. L., Campuzano-Jost, P., Perring, A., Schwarz, J.,
1198 Markovic, M. Z., Russell, P., Redemann, J., Shinzuka, Y., Streets, D. G., Yan, F., Dibb,
1199 J., Yokelson, R., Toon, O. B., Hyer, E., and Carmichael, G. R.: Revealing important

1200 nocturnal and day-to-day variations in fire smoke emissions through a novel
1201 multiplatform inversion, submitted.

1202 Sarwar, G., Simon, H., Fahey, K., Mathur, R., Goliff, W. S., and Stockwell, W. R.: Impact of
1203 sulfur dioxide oxidation by Stabilized Criegee Intermediate on sulfate, *Atmos. Environ.*,
1204 85, 204-214, doi:10.1016/j.atmosenv.2013.12.013, 2014.

1205 Saunders, S. M., Jenkin, M. E., Derwent, R. G., and Pilling, M. J.: Protocol for the development
1206 of the Master Chemical Mechanism, MCM v3 (Part A): Tropospheric degradation of
1207 non-aromatic volatile organic compounds, *Atmos. Chem. Phys.*, 3, 161-180,
1208 doi:10.5194/acp-3-161-2003, 2003.

1209 Scarino, A. J., Oband, M. D., Fast, J. D., Burton, S. P., Ferrare, R. A., Hostetler, C. A., Berg, L.
1210 K., Lefer, B., Haman, C., Hair, J. W., Rogers, R. R., Butler, C., Cook, A. L., and Harper,
1211 D. B.: Comparison of mixed layer heights from airborne high spectral resolution lidar,
1212 ground-based measurements, and the WRF-Chem model during CalNex and CARES,
1213 *Atmos. Chem. Phys.*, 14, 5547-5560, doi:10.5194/acp-14-5547-2014, 2014a.

1214 Scarino, A. J., Ferrare, R., Burton, S., Hostetler, C., Hair, J., Rogers, R., Berkoff, T., Collins, J.,
1215 Seaman, S., Cook, A., Harper, D., Sawamura, P., Randles, C., and daSilva, A.: Assessing
1216 aerosol mixed layer heights from the NASA LaRC airborne HSRL-2 during the
1217 DISCOVER-AQ Field Campaigns: Houston 2013, Abstract A31C-3040 presented at
1218 2014 Fall Meeting, AGU, San Francisco, Calif., 15-19 Dec, 2014b.

1219 Schwarz, J. P., Perring, A. E., Markovic, M. Z., Gao, R. S., Ohata, S., Langridge, J., Law, D.,
1220 McLaughlin, R., and Fahey, D. W.: Technique and theoretical approach for quantifying
1221 the hygroscopicity of black-carbon-containing aerosol using a single particle soot
1222 photometer, *J. Aeros. Sci.*, 81, 110-126, doi:10.1026/j.jaerosci.2014.11.009, 2015.

1223 Sipila, M., Jokinen, T., Berndt, T., Richters, S., Makkonen, R., Donahue, N. M., Mauldin III, R.
1224 L., Kurten, T., Paasonen, P., Sarnela, N., Ehn, M., Junninen, H., Rissanen, M. P.,
1225 Thornton, J., Stratmann, F., Herrmann, H., Worsnop, D. R., Kulmala, M., Kerminen, V.-
1226 M., and Petaja, T.: Reactivity of stabilize Criegee intermediates (sCIs) from isoprene and
1227 monoterpene ozonolysis toward SO₂ and organic acids, *Atmos. Chem. Phys.*, 14, 12143-
1228 12153, doi:10.5194/acp-14-12143-2014, 2014.

1229 Solomon, P. A., Crumpler, D., Flanagan, J. B., Jayanty, R. K. M., Rickman, E. E., and McDade
1230 C. E.: U.S. National PM_{2.5} Chemical Speciation Monitoring Networks – CSN and
1231 IMPROVE: Description of Networks, *J. Air Waste Manage. Assoc.*, 64(12), 1410-1438,
1232 doi:10.1080/10962247.2014.956904, 2014.

1233 Spracklen, D. V., Jimenez, J. L., Carslaw, K. S., Worsnop, D. R., Evans, M. J., Mann, G. W.,
1234 Zhang, Q., Canagaratna, M. J., Allan, J., Coe, H., McFiggans, G., Rap, A., and Forster,
1235 P.: Aerosol mass spectrometer constraint on the global secondary organic aerosol budget,
1236 *Atmos. Chem. Phys.*, 11, 12109-12136, doi:10.5194/acp-11-12109-2011, 2011.

1237 St. Clair, J. M., McCabe, D. C., Crounse, J. D., Steiner, U., and Wennberg, P. O.: Chemical
1238 ionization tandem mass spectrometer for the in situ measurement of methyl hydrogen
1239 peroxide, *Rev. Sci. Instrum.*, 81, 094102-094106, doi:10.1063/1.3480552, 2010.

1240 Stone, D., Blitz, M., Daubney, L., Howes, N. U., and Seakins, P.: Kinetics of CH₂OO reactions
1241 with SO₂, NO₂, NO, H₂O, and CH₃CHO as a function of pressure, *Phys. Chem. Chem.*
1242 *Phys.*, 16, 1139-1149, doi:10.1039/c3cp54391a, 2014.

1243 Surratt, J. D., Kroll, J. H., Kleindienst, T. E., Edney, E. O., Claeys, M., Sorooshian, A., Ng, N. L.,
1244 Offenberg, J. H., Lewandowski, M., Jaoui, M., Flagan, R. C., and Seinfeld, J. H.:
1245 Evidence for organosulfates in secondary organic aerosol, *Environ. Sci., Tech.*, 41, 517-
1246 527, doi:10.1021/es062081q, 2007.

1247 Theil, H.: A rank-invariant method of linear and polynomial regression analysis, *Proc. Kon. Ned.*
1248 *Akad. V. Wetensch. A*, 53, 386-392, 1950.

1249 Thomson, D. S., Schein, M. E., and Murphy, D. M.: Particle analysis by laser mass spectrometry
1250 WB-57F instrument overview, *Aerosol Sci. Technol.*, 33(1-2), 153-169,
1251 doi:10.1080/027868200410903, 2000.

1252 Thornhill, K. L., Chen, G., Dibb, J., Jordan, C. E., Omar, A., Winstead, E. L., Schuster, G.,
1253 Clarke, A., McNaughton, C., Scheur, E., Blake, D., Sachse, G., Huey, L. G., Singh, H. B.,
1254 and Anderson, B. E.: The impact of local sources and long-range transport on aerosol
1255 properties over the northeast U.S. region during INTEX-NA, *J. Geophys. Res.*, 113,
1256 D08201, doi:10.1029/2007JD008666, 2008.

1257 Toon, O. B., et al.: Planning, implementation, and scientific goals of the Studies of Emissions and
1258 Atmospheric Composition, Clouds, and Climate Coupling by Regional Surveys
1259 (SEAC⁴RS) field mission, in prep.

1260 Travis, K., et al.: Declining NO_x in the Southeast US and implications for ozone-NO_x-VOC
1261 chemistry, presented at the SEAC⁴RS Science Team Meeting, Pasadena, Calif., 28 Apr –
1262 1 May, 2015.

1263 Tsigaridis, K., Daskalakis, N., Kanakidou, M., Adams, P. J., Artaxo, P., Bahadur, R., Balkanski,
1264 Y., Bauer, S. E., Bellouin, N., Benedetti, A., Bergman, T., Berntsen, T. K., Beukes, J. P.,
1265 Bian, H., Carslaw, K. S., Chin, M., Curci, G., Diehl, T., Easter, R. C., Ghan, S. J., Gong,
1266 S. L., Hodzic, A., Hoyle, C. R., Iversen, T., Jathar, S., Jimenez, J. L., Kaiser, J. W.,

1267 Kirkevåg, A., Koch, D., Kokkola, H., Lee, Y. H., Lin, G., Liu, X., Luo, G., Ma, X.,
1268 Mann, G. W., Mihalopoulos, N., Morcrette, J.-J., Müller, J.-F., Myhre, G.,
1269 Myriokefalitakis, S., Ng, S., O'Donnell, D., Penner, J. E., Pozzoli, L., Pringle, K. J.,
1270 Russell, L. M., Schulz, M., Sciare, J., Seland, Ø., Shindell, D. T., Sillman, S., Skeie, R.
1271 B., Spracklen, D., Stavrakou, T., Steenrod, S. D., Takemura, T., Tiitta, P., Tilmes, S.,
1272 Tost, H., van Noije, T., van Zyl, P. G., von Salzen, K., Yu, F., Wang, Z., Wang, Z.,
1273 Zaveri, R. A., Zhang, H., Zhang, K., Zhang, Q., and Zhang, X.: The AeroCom evaluation
1274 and intercomparison of organic aerosol in global models, *Atmos. Chem. Phys.*, 14,
1275 10845-10895, doi:10.5194/acp-14-10845-2014, 2014.

1276 Turquety, S., Logan, J. A., Jacob, D. J., Hudman, R. C., Leung, F. Y., Heald, C. L., Yantosca, R.
1277 M., Wu, S., Emmons, L. K., Edwards, D. P., and Sachse, G.: Inventory of boreal fire
1278 emissions for North America in 2004: the importance of peat burning and pyro-
1279 convective injections, *J. Geophys. Res.*, 112(D12), D12S03, doi:10.1029/2006JD007281,
1280 2007.

1281 van Donkelaar, A., Martin, R. V., Brauer, M., Kahn, R., Levy, R., Verduzco, C., and Villeneuve,
1282 P. J.: Global estimates of ambient fine particulate matter concentrations from satellite-
1283 based aerosol optical depth: development and application, *Environ. Health Perspect.*,
1284 118(6), 847-855, doi:10.1289/ehp.0901623, 2010.

1285 van Donkelaar, A., Martin, R. V., Pasch, A. N., Szykman, J. J., Zhang, L., Wang, Y. X., and
1286 Chen, D.: Improving the accuracy of daily-satellite-derived ground-level fine aerosol
1287 concentration estimates for North America, *Environ. Sci. Technol.*, 46, 11971-11978,
1288 doi:10.1021/es3025319, 2012.

1289 van Donkelaar, A., Martin, R. V., Spurr, R. J. D., Drury, E., Remer, L. A., Levy, R. C., and
1290 Wang, J.: Optimal estimation for global ground-level fine particulate matter
1291 concentrations, *J. Geophys. Res. Atmos.*, 118, 5621-5636, doi:10.1002/jgrd.50479, 2013.

1292 van Donkelaar, A., Martin, R. V., Brauer, M., and Boys, B. L.: Use of satellite observations for
1293 long-term exposure assessment of global concentrations of fine particulate matter,
1294 *Environ. Health Perspect.*, 123(2), 135-143, doi:10.1289/ehp.1408646, 2015.

1295 Wagner, N. L., Brock, C. A., Angevine, W. M., Beyersdorf, A., Campuzano-Jost, P., Day, D. A.,
1296 de Gouw, J. A., Diskin, G. S., Gordon, T. D., Graus, M. G., Huey, G., Jimenez, J. L.,
1297 Lack, D. A., Liao, J., Liu, X., Markovic, M. Z., Middlebrook, A. M., Mikoviny, T.,
1298 Peischl, J., Perring, A. E., Richardson, M. S., Ryerson, T. B., Schwarz, J. P., Warneke,
1299 C., Welti, A., Wisthaler, A., Ziemba, L. D., and Murphy, D. M.: In situ vertical profiles
1300 of aerosol extinction, mass, and composition over the southeast United States during

1301 SENEX and SEAC4RS: Observations of a modest aerosol enhancement aloft, *Atmos.*
1302 *Chem. Phys. Discuss.*, 15, 3127-3172, doi:10.5194/acpd-15-3127-2015, 2015.

1303 Walker, J. M., Philip, S., Martin, R. V., and Seinfeld J. H.: Simulation of nitrate, sulfate, and
1304 ammonium aerosols over the United States, *Atmos. Chem. Phys.*, 12, 11213-11227,
1305 doi:10.5194/acp-12-11213-2012, 2012.

1306 Wang, J., Jacob, D. J., and Martin, S. T.: Sensitivity of sulfate direct climate forcing to the
1307 hysteresis of particle phase transitions, *J. Geophys. Res.*, 113, D11207,
1308 doi:10.1029/2007JD009368, 2008.

1309 Wang, Q., Jacob, D. J., Spackman, J. R., Perring, A. E., Schwarz, J. P., Moteki, N., Marais, E. A.
1310 Ge, C., Wang, J., and Barrett, S. R. H.: Global budget and radiative forcing of black
1311 carbon aerosol: Constraints from pole-to-pole (HIPPO) observations across the Pacific, *J.*
1312 *Geophys. Res. Atmos.*, 119, 195-206, doi:10.1002/2013JD020824, 2014.

1313 Warneke, C., and the SENEX science team: Instrumentation and measurement strategy for the
1314 NOAA SENEX aircraft campaign as part of the Southeast Atmosphere Study 2013, to be
1315 submitted to *Atmos. Meas. Tech. Discuss.*, 2015.

1316 Washenfelder, R., Attwood, A. R., Brock, C. A., Guo, H., Xu, L., Weber, R. J., Ng, N. L., Allen,
1317 H. M., Ayres, B., Baumann, K., Cohen, R. C., Draper, D. C., Duffey, K. C., Edgerton, E.,
1318 Fry, J. L., Hu, W. W., Jimenez, J. L., Palm, B. B., Romer, P., Stone, E. A., Wooldridge,
1319 P. J., and Brown, S. S.: Biomass burning dominates brown carbon absorption in the rural
1320 southeastern United States, *Geophys. Res. Lett.*, 42, 653-664,
1321 doi:10.1002/2014GL062444, 2015.

1322 Weber, R. J., Sullivan, A. P., Peltier, R. E., Russell, A., Yan, B., Zheng, M., de Gouw, J.,
1323 Warneke, C., Brock, C., Holloway, J. S., Atlas, E. L., and Edgerton, E.: A study of
1324 secondary organic aerosol formation in the anthropogenic-influenced southeastern United
1325 States, *J. Geophys. Res.*, 112, D13302, doi:10.1029/2007JD008408, 2007.

1326 Welz, O., Savee, J. D., Osborn, D. L., Vasu, S. S., Percival, C. J., Shallcross, D. E., and Taatjes,
1327 C. A.: Direct kinetic measurements of Criegee Intermediate (CH_2OO) formed by reaction
1328 of CH_2I with O_2 , *Science*, 335, 204-207, doi:10.1126/science.1213229, 2012.

1329 Wolfe, G. M., Hanisco, T. F., Arkinson, H. L., Bui, T. P., Crouse, J. D., Dean-Day, J.,
1330 Goldstein, A., Guenther, A., Hall, S. R., Huey, G., Karl, T., Kim, P. S., Liu, X., Marvin,
1331 M. R., Mikoviny, T., Misztal, P., Nguyen, T. B., Peischl, J., Pollack, I., Ryerson, T., St.
1332 Clair, J. M., Teng, A., Travis, K. R., Wennberg, P. O., Wisthaler, A., and Ullmann, K.:
1333 Airborne flux observations provide novel constraints on sources and sinks of reactive
1334 gases in the lower atmosphere, submitted to *Science*, 2015.

1335 WRAP: Western Regional Air Partnership, Development of 2000-04 Baseline Period and 2018
1336 Projection Year Emission Inventories, Prepared by Air Sciences, Inc. Project No. 178-8,
1337 2005.

1338 Xu, L., Kollman, M. S., Song, C., Shilling, J. E., and Ng, N. L.: Effects of NO_x on the volatility
1339 of secondary organic aerosol from isoprene photooxidation, *Environ. Sci. Technol.*, 48,
1340 2253-2262, doi:10.1021/es404842g, 2014.

1341 Yu, K., et al.: Impact of grid resolution on tropospheric chemistry simulation constrained by
1342 observations from the SEAC⁴RS aircraft campaign, presented at the SEAC⁴RS Science
1343 Team Meeting, Pasadena, Calif., 28 Apr – 1 May, 2015.

1344 Yu, S., Dennis, R. L., Bhave, P. V., and Ender, B. K.: Primary and secondary organic aerosols
1345 over the United States: estimates on the basis of observed organic carbon (OC) and
1346 elemental carbon (EC), and air quality modeled primary OC/EC ratios, *Atmos. Environ.*,
1347 38, 5257-5268, doi:10.1016/j.atmosenv.2004.02.064, 2004.

1348 Zhang, H., Hoff, R. M., and Engel-Cox, J. A.: The relation between Moderate Resolution
1349 Imaging Spectroradiometer (MODIS) aerosol optical depth and PM_{2.5} over the United
1350 States: a geographical comparison by U.S. Environmental Protection Agency regions, *J.*
1351 *Air Waste Manage. Assoc.*, 59:11, 1358-1369, doi:10.3155/1047-3289.59.11.1358, 2009.

1352 Zhang, L., Gong, S., Padro, J., and Barrie, L.: A size-segregated particle dry deposition scheme
1353 for an atmospheric aerosol module, *Atmos. Environ.*, 35, 549-560, doi:10.1016/s1352-
1354 2310(00)00326-5, 2001.

1355 Zhang, L., Jacob, D. J., Knipping, E. M., Kumar, N., Munger, J. W., Carouge, C. C., van
1356 Donkelaar, A., Wang, Y. X., and Chen, D.: Nitrogen deposition to the United States:
1357 distribution, sources, and processes, *Atmos. Chem. Phys.*, 12, 4539-4554,
1358 doi:10.5194/acp-12-4539-2012, 2012.

1359 Zhang, Q., Jimenez, J. L., Canagaratna, M. R., Allan, J. D., Coe, H., Ulbrich, I., Alfarra, M. R.,
1360 Takami, A., Middlebrook, A. M., Sun, Y. L., Dzepina, K., Dunlea, E., Docherty, K., De-
1361 Carlo, P. F., Salcedo, D., Onasch, T., Jayne, J. T., Miyoshi, T., Shimojo, A.,
1362 Hatakeyama, S., Takegawa, N., Kondo, Y., Schneider, J., Drewnick, F., Borrmann, S.,
1363 Weimer, S., Demerjian, K., Williams, P., Bower, K., Bahreini, R., Cottrell, L., Griffin,
1364 R. J., Rautiainen, J., Sun, J. Y., Zhang, Y. M., and Worsnop, D. R.: Ubiquity and
1365 dominance of oxygenated species in organic aerosols in anthropogenically-influenced
1366 Northern Hemisphere midlatitudes, *Geophys. Res. Lett.*, 34, 6, L13801,
1367 doi:10.1029/2007gl029979, 2007.

1368 Zhang, X., Liu, Z., Hecobian, A., Zheng, M., Frank, N. H., Edgerton, E. S., and Weber, R. J.:
1369 Spatial and seasonal variations of fine particle water-soluble organic carbon (WSOC)
1370 over the southeastern United States: implications for secondary organic aerosol
1371 formation, *Atmos. Chem. Phys.*, 12, 6593-6607, doi:10.5194/acp-12-6593-2012, 2012.
1372 Zhu, L., et al.: Indirect validation of new OMI, GOME-2, and OMPS formaldehyde (HCHO)
1373 retrievals using SEAC⁴RS data, presented at the SEAC⁴RS Science Team Meeting,
1374 Pasadena, Calif., 28 Apr – 1 May, 2015.
1375 Zotter, P., El-Haddad, I., Zhang, Y., Hayes, P. L., Zhang, X., Lin, Y.-H., Wacker, L., Schnelle-
1376 Kreis, J., Abbaszade, G., Zimmerman, R., Surratt, J. D., Weber, R., Jimenez, J. L., Szidat,
1377 S., Baltensperger, U., and Prevot, A. S. H.: Diurnal cycle of fossil and nonfossil carbon
1378 using radiocarbon analyses during CalNex, *J. Geophys. Res. Atmos.*, 119, 6818-6835,
1379 doi:10.1002/2013JD021114, 2014.
1380
1381
1382
1383
1384
1385
1386
1387
1388
1389
1390
1391
1392
1393
1394
1395
1396
1397
1398
1399
1400
1401

1402 **Tables**

1403

1404 Table 1: Contiguous US (CONUS) Emissions for 2013^a

Source	NO _x [Tg N]	CO [Tg]	SO ₂ [Tg S]	NH ₃ [Tg]	BC [Tg]	OC [Tg]	Isoprene ^b [Tg C]	Monoterpenes ^b [Tg C]
Anthropogenic ^c	2.7 (0.07)	29.8 (0.65)	2.8 (0.14)	3.5 ^d (0.11)	0.26 (0.008)	0.58 (0.01)	-	-
Open Fires ^e	0.14 (0.004)	7.9 (0.21)	0.13 (0.002)	0.44 (0.008)	0.19 (0.003)	0.93 (0.01)	-	-
Soil ^f	0.69 (0.03)	-	-	-	-	-	-	-
Vegetation	-	-	-	0.17 (0.002)	-	-	12.2 (2.2)	4.1 (0.5)
Total	3.5 (0.11)	37.7 (0.85)	2.9 (0.14)	4.1 (0.12)	0.45 (0.01)	1.5 (0.02)	12.2 (2.2)	4.1 (0.5)

1405

1406 ^aAnnual totals. Emissions in the Southeast US for the two-month SEAC⁴RS period (August-
1407 September) are shown in parentheses. The Southeast US domain is as defined in Figure 2.

1408 ^bBiogenic VOC emissions are from the MEGAN2.1 inventory (Guenther et al., 2012) with
1409 isoprene emissions decreased by 15% (see text).

1410 ^cAnthropogenic emissions are from the EPA National Emissions Inventory (NEI08v2) scaled
1411 nationally to 2013 and with additional adjustments described in the text.

1412 ^dAgricultural ammonia emissions are from the MASAGE inventory on a 2° x 2.5° grid (Paulot et
1413 al., 2014), and are distributed on the 0.25° x 0.3125° grid following NEI08v2 as described in the
1414 text.

1415 ^eOpen fire emissions are from the Quick Fire Emissions Dataset (Darmenov and da Silva, 2013),
1416 with adjustments described in the text.

1417 ^fSoil and fertilizer NO_x emissions are from the BDSNP algorithm (Hudman et al., 2012).
1418 Fertilizer emissions are included in the anthropogenic total.

1419

1420

1421

1422

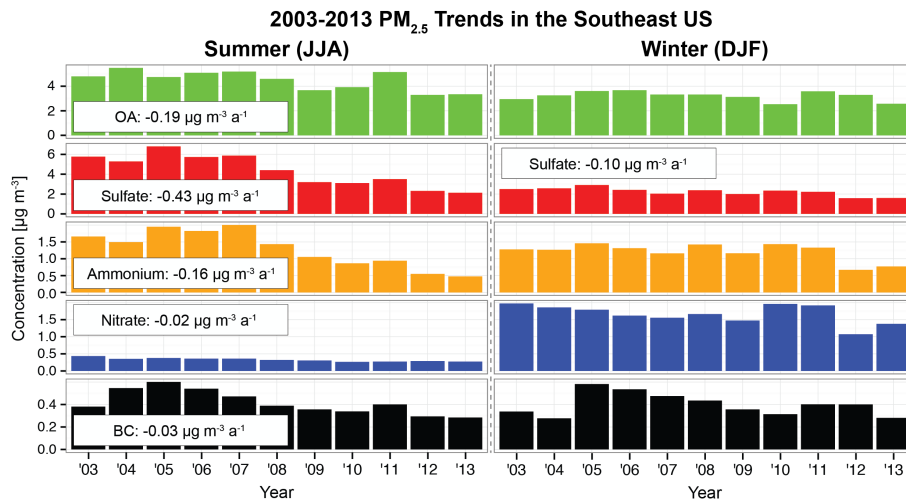
1423

1424

1425

1426 Figures

1427



1428

1429

1430 Figure 1: Summertime and wintertime trends in mean surface PM_{2.5} in the Southeast US for 2003-
1431 2013. Seasonal averages for each component are calculated by combining data from the EPA
1432 CSN and IMPROVE networks over the Southeast US domain defined in Figure 2. Ammonium is
1433 only measured by CSN. Organic aerosol (OA) and black carbon (BC) are only from IMPROVE
1434 because of change in the CSN measurement protocol over the 2003-2013 period and differences
1435 in the OA measurements between the two networks (see text for details). OA is inferred here
1436 from measured organic carbon (OC) using an OA/OC mass ratio of 2.24 as measured by the
1437 Aerodyne Aerosol Mass Spectrometer (AMS) in the boundary layer over the Southeast US. Note
1438 the different scales in different panels (sulfate and OA contribute most of PM_{2.5}). Trends are
1439 calculated using the Theil-Sen estimator (Theil, 1950) and are shown only if significant at the $\alpha =$
1440 0.05 level. Only the sulfate trend is significant in winter.

1441

1442

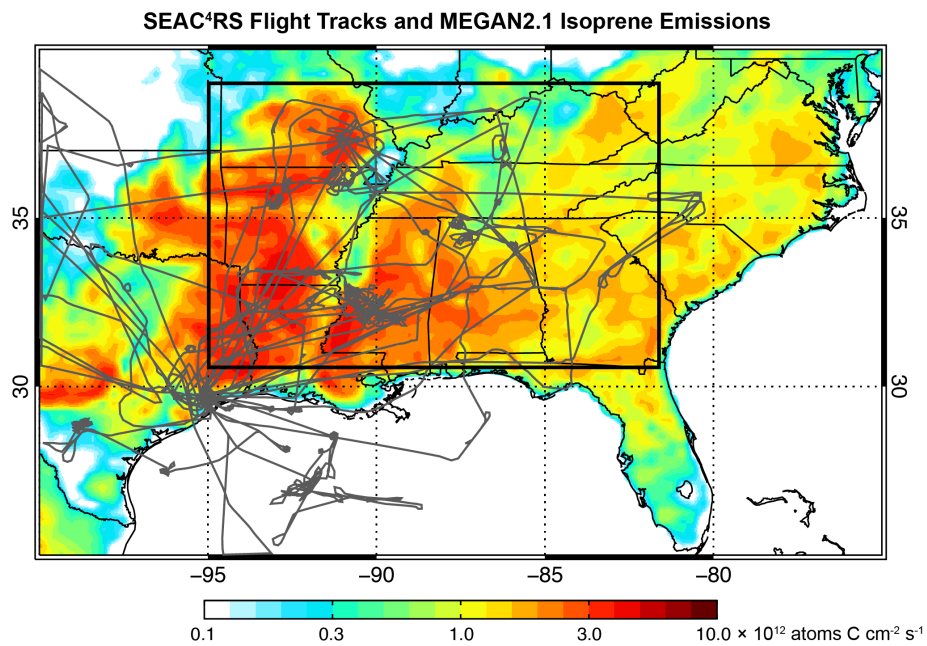
1443

1444

1445

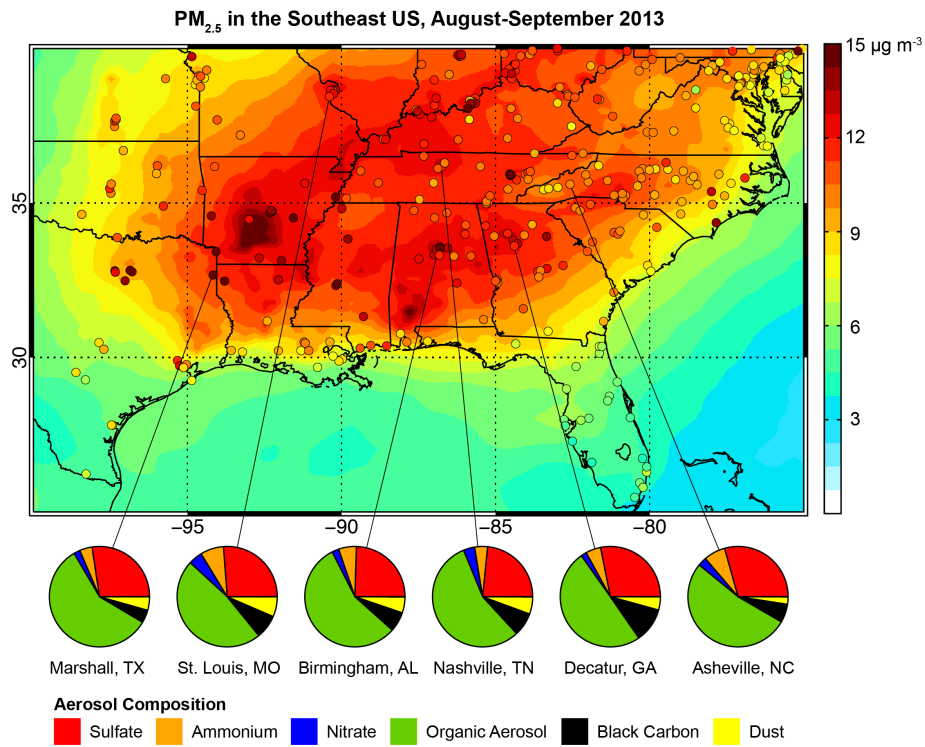
1446

1447



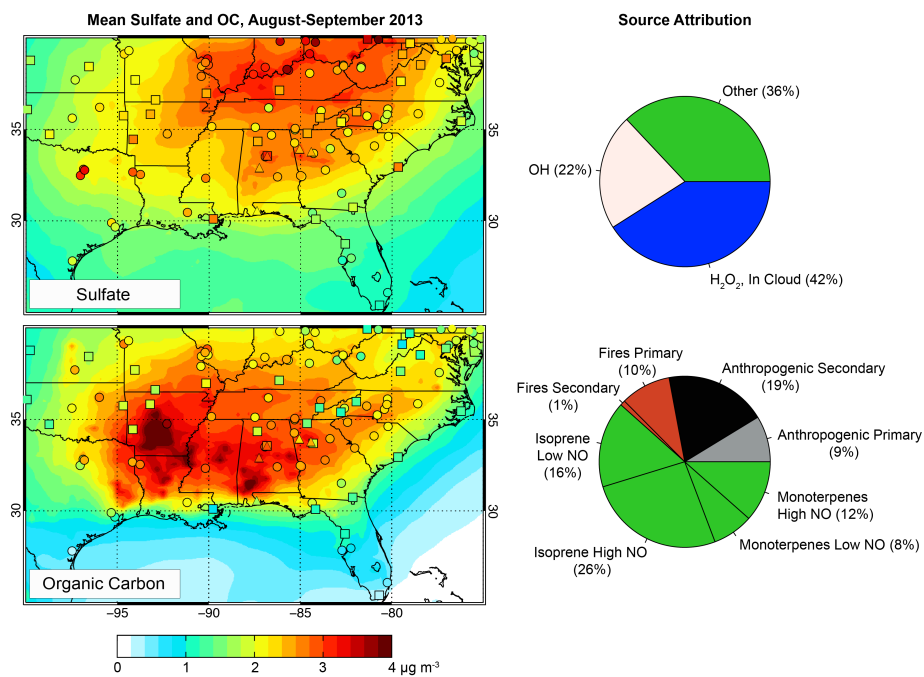
1448
 1449
 1450
 1451
 1452
 1453
 1454
 1455
 1456
 1457
 1458
 1459
 1460
 1461
 1462
 1463
 1464
 1465

Figure 2: Flight tracks of the DC-8 aircraft during SEAC⁴RS superimposed on mean MEGAN2.1 isoprene emissions for August-September 2013. The thick black line delineates the Southeast US domain as defined in this paper [95° W – 81.5° W, 30.5° N – 39° N].



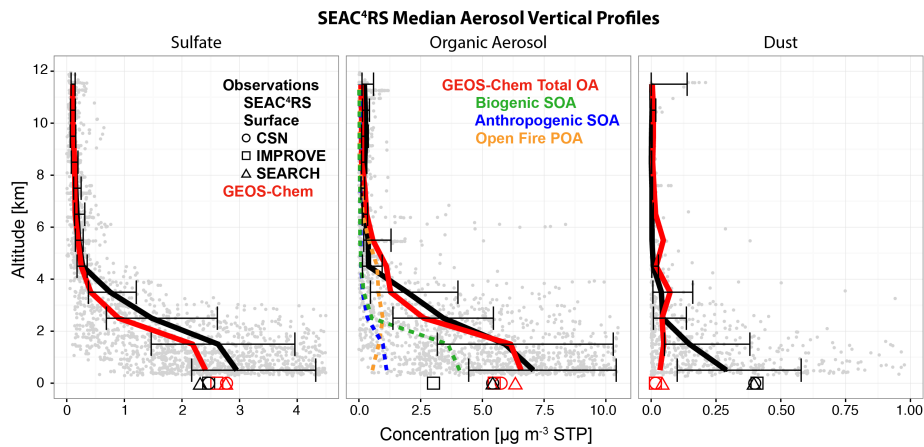
1466
 1467
 1468
 1469
 1470
 1471
 1472
 1473
 1474
 1475
 1476
 1477
 1478
 1479
 1480
 1481

Figure 3: Mean PM_{2.5} in the Southeast US in August-September 2013. EPA observations (circles) are compared to GEOS-Chem model values (background). Model values are calculated at 35% relative humidity as per the Federal Reference Method protocol. Observed mean PM_{2.5} speciation by mass is shown in the pie charts for representative CSN sites. Organic aerosol (OA) mass concentrations are derived from measurements of organic carbon (OC) by assuming an OA/OC mass ratio of 2.24.



1482
 1483
 1484
 1485
 1486
 1487
 1488
 1489
 1490
 1491
 1492
 1493
 1494
 1495
 1496
 1497
 1498
 1499

Figure 4: Mean sulfate (top) and OC (bottom) surface air concentrations in the Southeast US in August-September 2013. Network observations from CSN (circles), IMPROVE (squares), and SEARCH (triangles) are compared to GEOS-Chem model values (background). OC measurements are artifact-corrected as described in the text. Source attribution for sulfate and OC is shown at right as averages for the Southeast US domain defined in Figure 2. For sulfate, source attribution is by SO₂ oxidant. For OC, source attribution is primary or secondary, by source type, and by NO regime.



1500

1501

1502 Figure 5: Median vertical profiles of aerosol concentrations over the Southeast US (Figure 2)
 1503 during the SEAC⁴RS aircraft campaign (August-September 2013). Observed and simulated
 1504 profiles of sulfate (left), OA (center), and dust (right) in 1-km bins are shown with the
 1505 corresponding median surface network observations. OC from the surface networks is converted
 1506 to OA using an OA/OC ratio of 2.24. The contributions of anthropogenic SOA, biogenic SOA,
 1507 and open fire POA to total simulated OA are also shown. The individual observations are shown
 1508 in gray and the horizontal bars denote the 25th and 75th percentiles of the observations.
 1509 Concentrations are in $\mu\text{g m}^{-3}$ converted to STP conditions for the aircraft data and under local
 1510 conditions for the surface data. The choice of scale truncates some very large individual
 1511 observations.

1512

1513

1514

1515

1516

1517

1518

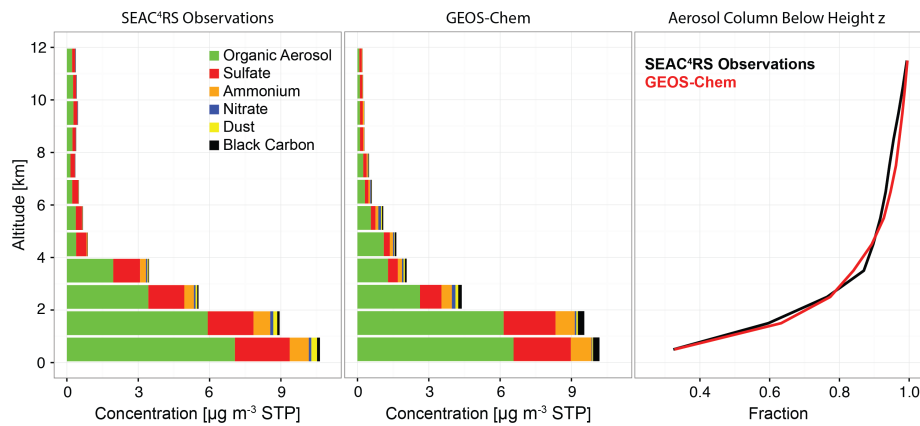
1519

1520

1521

1522

1523



1524

1525

1526 Figure 6: Median vertical profiles of aerosol composition over the Southeast US during
 1527 SEAC⁴RS (August-September 2013). Observations from the DC-8 aircraft (left) are compared to
 1528 GEOS-Chem values sampled at the aircraft times and locations (center). Also shown is the
 1529 observed and simulated fraction of the total aerosol mass column below a given height (right).
 1530 The Southeast US domain is as defined in Figure 2.

1531

1532

1533

1534

1535

1536

1537

1538

1539

1540

1541

1542

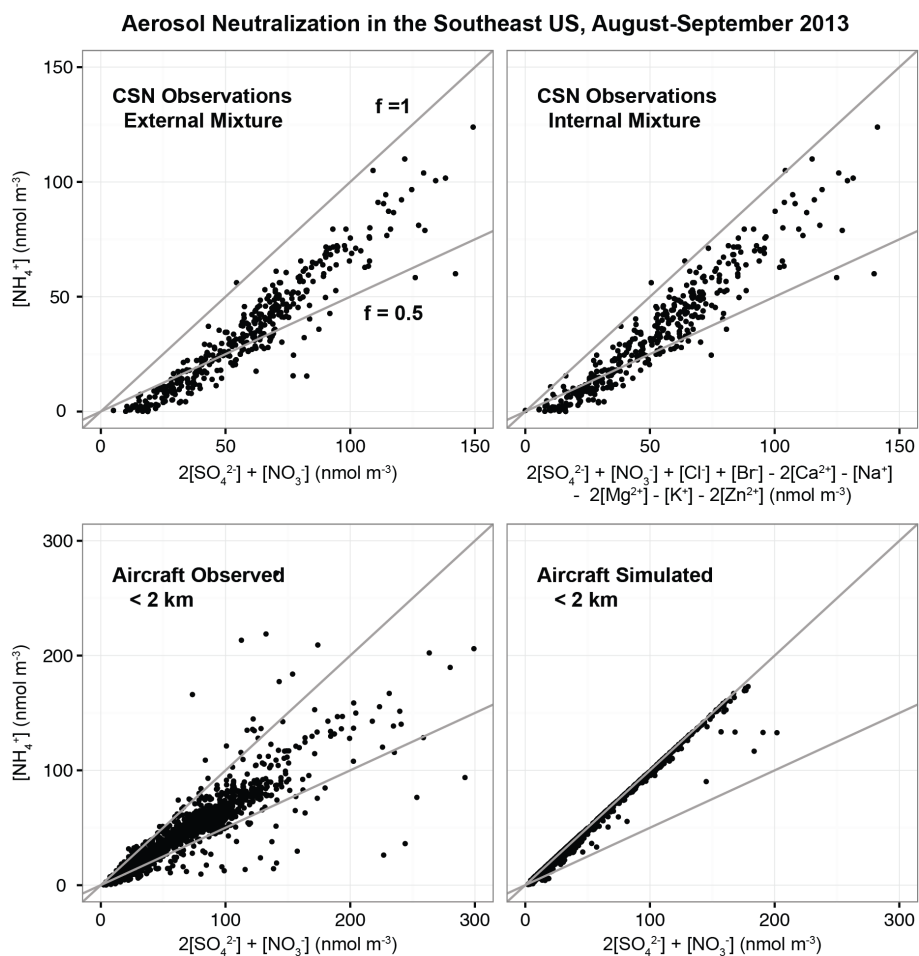
1543

1544

1545

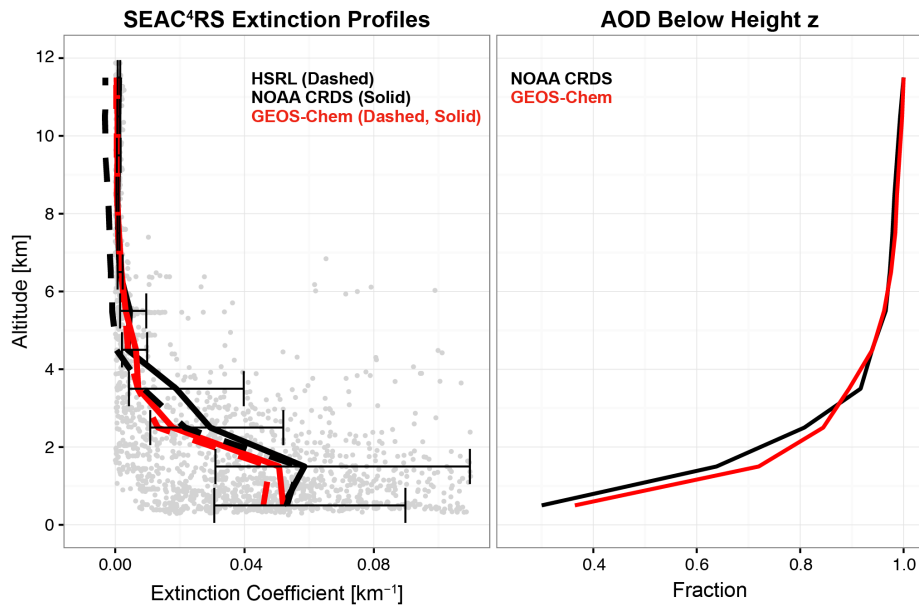
1546

1547



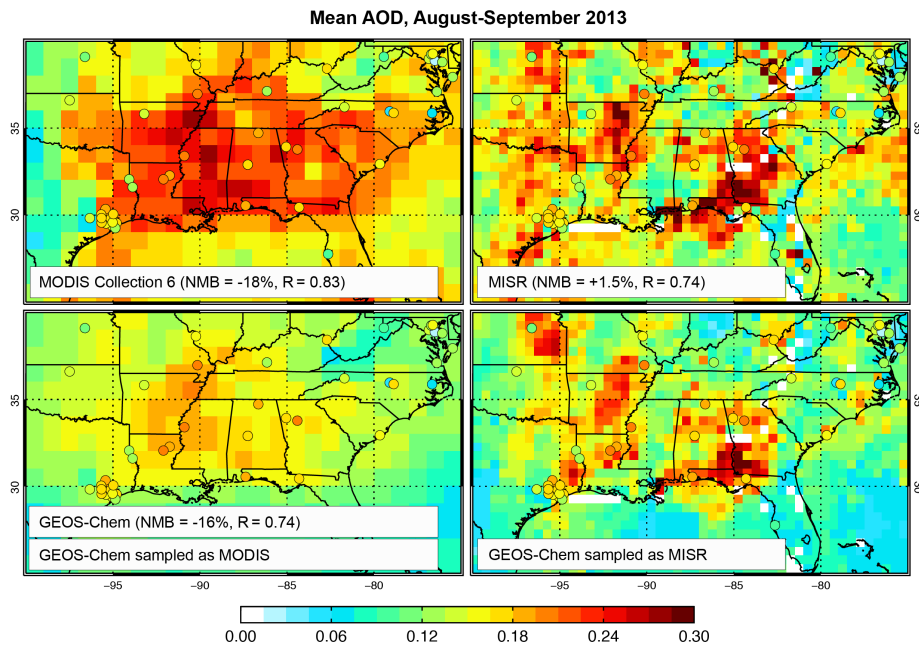
1548
1549

1550 Figure 7: Extent of neutralization of sulfate aerosol in the Southeast US (August-September
1551 2013). The extent of neutralization for an external sulfate-nitrate-ammonium (SNA) mixture is
1552 given by the $f = [\text{NH}_4^+] / (2[\text{SO}_4^{2-}] + [\text{NO}_3^-])$ molar ratio, and this can be adjusted for an internal
1553 mixture by considering additional ions. The top panels show observations from the CSN network
1554 assuming an external (left) or internal (right) mixture; there is little difference between the two
1555 because the concentrations of additional ions are usually small. The bottom panels show the
1556 SEAC⁴RS aircraft observations below 2 km and corresponding GEOS-Chem values. Also shown
1557 are the lines corresponding to different extents of neutralization ($f = 0.5$ for ammonium bisulfate
1558 and $f = 1$ for ammonium sulfate).



1559
 1560
 1561
 1562
 1563
 1564
 1565
 1566
 1567
 1568
 1569
 1570
 1571
 1572
 1573
 1574
 1575
 1576
 1577
 1578

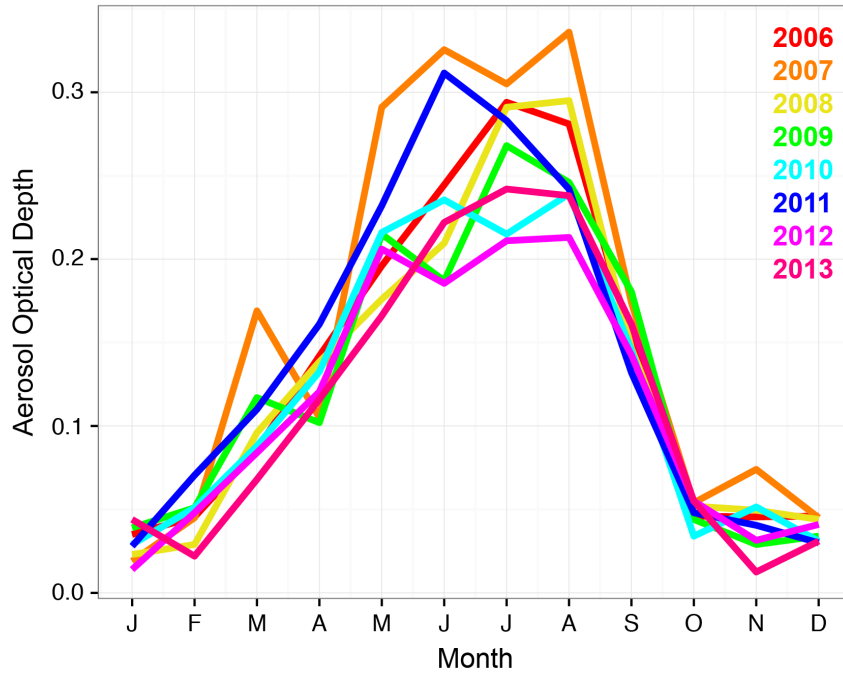
Figure 8: Median vertical profiles of aerosol extinction coefficients (532 nm) over the Southeast US during SEAC⁴RS. The left panel shows independent observations from the NASA HSRL and NOAA CRDS instruments, with GEOS-Chem sampled at the times and locations of the available instrument data. The individual CRDS observations are shown in gray and the horizontal bars denote the 25th and 75th percentiles of the CRDS observations for each 1-km bin. The choice of scale truncates some very large individual observations. The right panel shows the observed (CRDS) and simulated fraction of the total AOD below a given height. The Southeast US domain is as defined in Figure 2.



1579
 1580
 1581
 1582
 1583
 1584
 1585
 1586
 1587
 1588
 1589
 1590
 1591
 1592
 1593
 1594
 1595
 1596
 1597

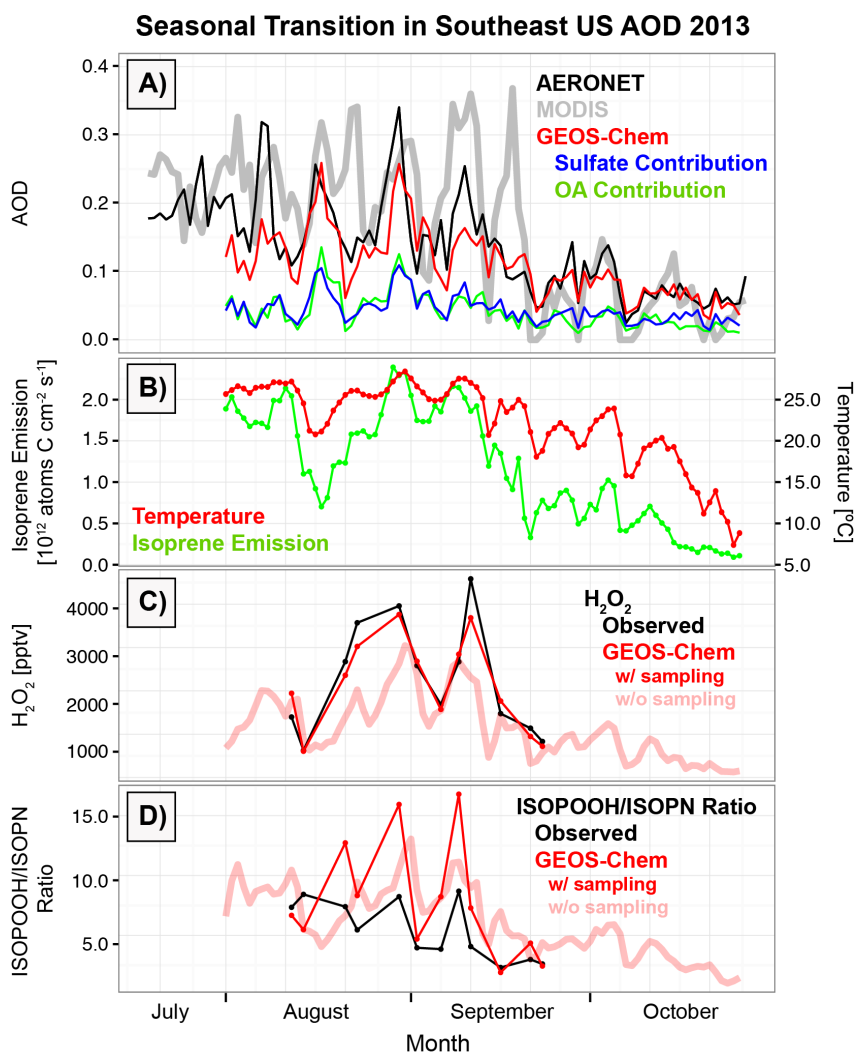
Figure 9: Mean aerosol optical depths (AODs) over the Southeast US during SEAC⁴RS (August-September 2013). AERONET data are shown as circles and are the same in all panels. The top panels show MODIS and MISR satellite observations with comparison statistics to AERONET (correlation coefficients, numerical mean biases or NMBs of collocated observations in time and space). The bottom panels show GEOS-Chem model values sampled at the same locations and times as the satellite retrievals. The noise in the MISR panels reflects infrequent sampling (9-day return time, compared to 1-day for MODIS). The negative NMB for the MODIS data reflects occasional retrievals of negative AOD.

MODIS AOD in the Southeast US, 2006-2013



1598
1599
1600
1601
1602
1603
1604
1605
1606
1607
1608
1609
1610
1611
1612
1613
1614

Figure 10: Seasonal variation of MODIS AOD over the Southeast US for 2006-2013. The Southeast US domain is as defined in Figure 2.



1615
1616

1617 Figure 11: Seasonal transition of aerosol optical depth (AOD) and related variables over the
1618 Southeast US in August-October 2013. (A) AODs measured by MODIS and AERONET, and
1619 GEOS-Chem values sampled at AERONET times and locations with simulated contributions
1620 from sulfate and OA. (B) 24-h average MEGAN2.1 isoprene emissions and GEOS-FP surface air
1621 temperatures. (C) H₂O₂ concentrations measured from the aircraft below 1 km altitude and
1622 simulated by GEOS-Chem sampled at the times and locations of the observations. Each data
1623 point represents the median value over the Southeast US for an individual flight. GEOS-Chem

1624 H₂O₂ concentrations averaged over the entire region (i.e. without sampling along the flight tracks)
1625 are shown separately and extend into October. (D) Same as (C) but for the molar ratio of isoprene
1626 peroxides (ISOPOOH) to isoprene nitrates (ISOPN). The Southeast US domain is as defined in
1627 Figure 2.

1628

1629

1630

1631

1632

1633

1634

1635

1636

1637

1638

1639

1640

1641

1642

1643

1644

1645

1646

1647

1648

1649

1650

1651

1652

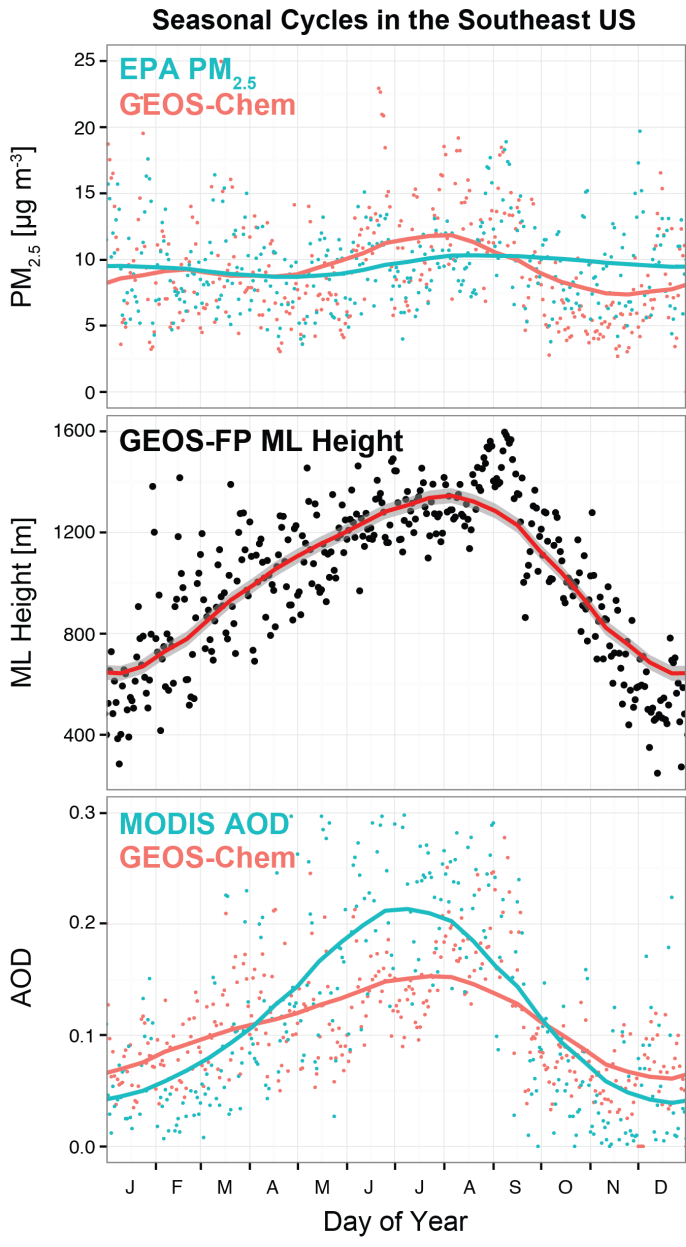
1653

1654

1655

1656

1657



1658

1659

1660 Figure 12: Seasonal aerosol cycle in the Southeast US in 2013. (Top) Daily mean EPA and

1661 GEOS-Chem $PM_{2.5}$. (Middle) Daily maximum mixed layer height from GEOS-FP with 40%

1662 downward correction applied year-round as in GEOS-Chem (see Section 2). (Bottom) Daily
1663 mean AOD from MODIS and GEOS-Chem. GEOS-Chem results in this figure are from the
1664 coarse-resolution ($4^\circ \times 5^\circ$) global simulation for 2013. Smoothed curves are calculated using a
1665 low-pass filter. All values are averaged over the Southeast US as defined in Figure 2.